










## Article

# Assessment of Extracellular Particles Directly in Diluted Plasma and Blood by Interferometric Light Microscopy. A Study of 613 Human and 163 Canine Samples

Boštjan Korenjak <sup>1</sup>, Armando Tratenšek <sup>2</sup>, Matevž Arko <sup>1</sup>, Anna Romolo <sup>1</sup>, Matej Hočevar <sup>3</sup>, Matic Kisovec <sup>4</sup>, Maxence Berry <sup>1,5</sup>, Apolonija Bedina Zavec <sup>4</sup>, David Drobne <sup>6,7</sup>, Tomaž Vovk <sup>2</sup>, Aleš Iglič <sup>8</sup>, Alenka Nemeč Svete <sup>9</sup>, Vladimira Erjavec <sup>9</sup> and Veronika Kralj-Iglič <sup>1,\*</sup>

<sup>1</sup> University of Ljubljana, Faculty of Health Sciences, Laboratory of Clinical Biophysics, SI-1000 Ljubljana, Slovenia; bostjan.korenjak@zf.uni-lj.si (B.K.); matevz.arko@zf.uni-lj.si (M.A.); anna.romolo@zf.uni-lj.si (A.R.); maxence.berry@etu.univ-poitiers.fr (M.B.)

<sup>2</sup> University of Ljubljana, Faculty of Pharmacy, SI-1000 Ljubljana, Slovenia; armando.tratensek@ffa.uni-lj.si (A.T.); tomaz.vovk@ffa.uni-lj.si (T.V.)

<sup>3</sup> Institute of Metals and Technology, SI-1000 Ljubljana, Slovenia; matej.hocevar@imt.si

<sup>4</sup> National Institute of Chemistry, SI-1000 Ljubljana, Slovenia; matic.kisovec@ki.si (M.K.); polona.bedina@ki.si (A.B.Z.)

<sup>5</sup> College for Basic and Applied Sciences, University of Poitiers, 86000 Poitiers, France

<sup>6</sup> Department of Gastroenterology, University Medical Centre Ljubljana, SI-1000 Ljubljana, Slovenia; david.drobne@kclj.si

<sup>7</sup> University of Ljubljana, Faculty of Medicine, SI-1000 Ljubljana, Slovenia

<sup>8</sup> University of Ljubljana, Faculty of Electrical Engineering, Laboratory of Physics, SI-1000 Ljubljana, Slovenia; ales.iglic@fe.uni-lj.si

<sup>9</sup> University of Ljubljana, Veterinary Faculty, Small Animal Clinic, SI-1000 Ljubljana, Slovenia; alenka.nemecsvete@vf.uni-lj.si (A.N.S.); vladimira.erjavec@vf.uni-lj.si (V.E.)

\* Correspondence: veronika.kralj-iglic@zf.uni-lj.si; Tel.: +386-4172-0766



**Citation:** Korenjak, B.; Tratenšek, A.; Arko, M.; Romolo, A.; Hočevar, M.; Kisovec, M.; Berry, M.; Bedina Zavec, A.; Drobne, D.; Vovk, T.; et al. Assessment of Extracellular Particles Directly in Diluted Plasma and Blood by Interferometric Light Microscopy. A Study of 613 Human and 163 Canine Samples. *Cells* **2024**, *13*, 2054. <https://doi.org/10.3390/cells13242054>

Academic Editor: Péter Viktor Nagy

Received: 30 September 2024

Revised: 24 October 2024

Accepted: 29 October 2024

Published: 12 December 2024



**Copyright:** © 2024 by the authors. Licensee MDPI, Basel, Switzerland. This article is an open access article distributed under the terms and conditions of the Creative Commons Attribution (CC BY) license (<https://creativecommons.org/licenses/by/4.0/>).

**Abstract:** Extracellular nanoparticles (EPs) are a subject of increasing interest for their biological role as mediators in cell–cell communication; however, their harvesting and assessment from bodily fluids are challenging, as processing can significantly affect samples. With the aim of minimizing processing artifacts, we assessed the number density ( $n$ ) and hydrodynamic diameter ( $D_h$ ) of EPs directly in diluted plasma and blood using the following recently developed technique: interferometric light microscopy (ILM). We analyzed 613 blood and plasma samples from human patients with inflammatory bowel disease (IBD), collected in trisodium citrate and ethylenediaminetetraacetic acid (EDTA) anticoagulants, and 163 blood and plasma samples from canine patients with brachycephalic obstructive airway syndrome (BOAS). We found a highly statistically significant correlation between  $n$  in the plasma and  $n$  in the blood only in the human (i.e., but not canine) blood samples, between the samples with trisodium citrate and EDTA, and between the respective  $D_h$  for both species (all  $p < 10^{-3}$ ). In the human plasma, the average  $\langle D_h \rangle$  was  $139 \pm 31$  nm; in the human blood,  $\langle D_h \rangle$  was  $158 \pm 11$  nm; in the canine plasma,  $\langle D_h \rangle$  was  $155 \pm 32$  nm; and in the canine blood,  $\langle D_h \rangle$  was  $171 \pm 33$  nm. The differences within species were statistically significant ( $p < 10^{-2}$ ), with sufficient statistical power ( $P > 0.8$ ). For  $\langle n \rangle$ , we found no statistically significant differences between the human plasma and blood samples or between the samples with trisodium citrate and EDTA. Our results prove that measuring  $n$  and  $D_h$  of EPs in minimally processed fresh blood and in diluted fresh plasma by means of ILM is feasible for large populations of samples.

**Keywords:** extracellular particles; extracellular vesicles; exosomes; membrane vesiculation; platelets; blood products; platelet-rich plasma; liquid biopsy; membrane enclosed; drug delivery

## 1. Introduction

Blood and plasma contain cells, soluble proteins, such as albumin, immunoglobulin, fibrinogen, lipoprotein, and ribonucleoprotein aggregates, and nano-sized extracellular particles (EPs). In 1976, a report on harvesting platelet-derived EPs presented electron microscope images of EPs and of activated platelets undergoing budding [1]. It was indicated that EPs could have biological effects, thereby implying their potential roles in diagnostics and therapy [1]. Since then, numerous studies on blood EPs have been performed, and knowledge of EPs' physicochemical properties, morphology, and specific biological effects has accumulated ([2–4] and included references). Here, we focus on ex vivo blood EPs and plasma EPs.

EPs mediate intercellular communication by exchanging the material and information stored within cellular fragments [3,4]. They travel to a recipient cell where the EPs' cargoes (including proteins and various types of nucleic acids and their fragments) can be internalized. By activating remote cellular processes, EPs become the effectors of systemic metabolic regulation [5]. In samples, EPs are considered potential indicators of the body's clinical status, in particular, its response to disease. They have been isolated from diverse bodily fluids, including cerebrospinal fluid, breast milk, semen, urine, saliva, amniotic fluid, ascites, bile, and blood [3], as well as from plants [6].

The basic required information about EPs includes the identity (indicated by the shape and ultrastructure), number density ( $n$ ), and size in vivo. However, with currently available methods, blood EPs cannot be assessed in vivo, and sampling should be performed prior to their observation and characterization. The most widely used methods are (differential) ultracentrifugation (UC), size-exclusion chromatography (SEC), filtration, precipitation, and capture by affinity structures [4].

EPs are relatively small particles (smaller than 1  $\mu\text{m}$ , down to tens of nanometers). Because of resolution limits, they cannot be visualized live using an optical microscope. Scanning electron microscopy (SEM) [7–10] and transmission electron microscopy (TEM) [11–14] provide information on the identity, shape, and size of EPs. Cryogenic TEM (cryoTEM) also shows the ultrastructure of EPs [15,16]. In samples, EPs are numerous, and batch methods provide information on the population of EPs in a sample. Flow cytometry (FCM) is used to assess the number density of EPs ( $n$ ) and their distribution [17–19]. Dynamic light scattering (DLS) provides the mean hydrodynamic diameter of EPs ( $D_h$ ); the dispersity index and the intensity of scattered light that accounts for the abundance of EPs [20,21] and, in combination with static light scattering, yields the radius of gyration ( $R_g$ ), which enables the determination of the structural factor  $R_g/R_{h,0}$  (where  $R_h = D_h/2$ ) [22,23]. Nanotracking analysis (NTA) [24,25] and interferometric light microscopy (ILM) [26–29] are used to determine both  $n$  and  $D_h$ . Tunable resistive pulse sensing (TRPS) [30–33] is based on changes in the electric current in which the EPs are participating and yields their  $n$  and size. Nanostructural information on highly monodispersed and concentrated EP samples can be acquired by small-angle X-ray scattering (SAXS) [34].

Batch methods are unable to distinguish different types of EPs in samples that have similar sizes and physical properties but differ in their origins and compositions [35]. Furthermore, experimental evidence indicates that the methods used to harvest and assess EPs significantly influence the content of samples [36]. To obtain plasma from blood, erythrocytes are sedimented, usually by means of centrifugation. Although the centripetal acceleration of the centrifuge rotor required to produce plasma is moderate, blood cells are affected [37]. Blood manipulation may promote cell vesiculation, vesicle fragmentation, or fusion, as well as interactions with other particles in a sample and with the material in contact with the sample. This can affect the configuration of a sample. It is likely that in blood preparations, the populations of particles acquired and measured using different methods are, to a large extent, diverse. This is particularly detrimental for their potential use in clinics, as information about the characteristics of the samples that may reflect the clinical status of the blood donor can be altered because of processing.

A possible aspect would be to avoid processing samples as much as possible. In light of this aim, FCM was applied to assess  $n$  of EPs directly in diluted blood from 22 healthy subjects [38], and in 56 patients with pancreatic cancer and 48 healthy controls [39]. Marchisio et al. (2021) sorted fluorescent-dyed EVs according to their markings [38], and Brocco et al. (2022) related  $n$  to the clinical status of the patients [39]. EPs were assessed in plasma without prior isolation—by DLS [20,40], NTA [35,41], TRPS [41,42], and FCM [43]. Božič et al. (2019) assessed the average  $D_h$  of EPs in diluted and filtered plasma samples from three healthy donors [22]. Kogej et al. (2021) applied the method proposed by Božič et al. (2019) to diluted and filtered plasma samples from seven patients with ovarian cancer, seven controls, and two patients with other diseases [23]. In a pilot study, Berry et al. (2024) measured  $D_h$  of EPs in 250 diluted plasma samples from multiple species (canine, equine, and human) by ILM [44].

The methods that show promise for clinical applications should prove feasible for larger populations of samples. Following agreement between the results obtained by DLS and ILM on a small number of various samples [28] and in a preliminary multispecies study [44], in this work we report on the assessment of  $n$  and  $D_h$  by ILM in the following two larger populations involved in ongoing clinical studies: human patients with IBD and canine patients with BOAS.

## 2. Materials and Methods

Information regarding the sample preparation is documented in the MIBlood-EV reports.

### 2.1. Human Patients

The observational study included 74 patients (35 females and 39 males) diagnosed with inflammatory bowel disease (39 with Crohn's disease and 35 with ulcerative colitis). The median age of the cohort was 46 years (interquartile range [IQR] 31–59 years), the median height was 172 cm (IQR 165–179 cm), and the median weight was 72 kg (IQR 62–84 kg). The study participants were outpatients at the University Medical Center Ljubljana, starting a new biological treatment at the time of inclusion in the study. Patients were followed for 6 months, during which multiple samples were collected for analysis, including 166 samples of plasma with trisodium citrate and 154 samples of each of the following: plasma with EDTA, blood with trisodium citrate, and blood with EDTA (altogether 613 samples). The study was approved by the National Medical Ethics Committee of the Republic of Slovenia (0120-271/2022/4; KME 27 July 2022).

### 2.2. Canine Patients

The study was conducted at the Small Animal Clinic of the Veterinary Faculty, University of Ljubljana, Slovenia, from March 2023 to August 2024. Seventy-six privately owned brachycephalic dogs were included in the study. The inclusion criteria were as follows: no coexisting systemic diseases, no medical treatment or vaccination within the previous month, a diagnosis of brachycephalic obstructive airway syndrome (BOAS), and no previous upper airway surgery. The diagnosis of BOAS was based on clinical signs and clinical examination and confirmed with an endoscopic examination of the upper airways. All dogs included in the study presented with severe multilayer upper airway obstruction and were classified as BOAS+ [45]. Patients were then followed for one year, during which, for some dogs, another set of samples was collected. Eighty-eight samples of each of the following were included: plasma with EDTA and blood with EDTA (altogether 176 samples). Formal written informed consent was obtained from the owners before the dogs participated in the study. All procedures in the study complied with the relevant Slovenian government regulations (Animal Protection Act, Official Gazette of the Republic of Slovenia, No. 43/2007). The study was approved by the Animals in Experiments Welfare Commission of the Veterinary Faculty, University of Ljubljana, approval number: 18-3/2022-1.

### 2.3. Blood Sampling in Human Patients

Blood was collected in the morning hours during regular ambulatory visits. A G21 needle (Microlance, Becton Dickinson, Plymouth, UK) and a 3.6 mL evacuated tube with trisodium citrate (Vacutube<sup>®</sup>, 9NC, LT Burnik, Ltd., Komenda, Slovenia) or 6 mL evacuated tube with potassium EDTA (BD Vacutainers<sup>®</sup>, 367864, Becton Dickinson, Plymouth, UK) were used. Samples were then transported to the laboratory (by bicycle (ca. 3 km)) where plasma preparation and dilution of the plasma and blood took place.

### 2.4. Blood Sampling in Canine Patients

Collection occurred in the morning after fasting for a minimum of 15 h overnight. A G21 needle (Microlance, Becton Dickinson, Franklin Lakes, NJ, USA) and 2 mL evacuated tubes with EDTA (Vacuette, Greiner Bio-One, Kremsmunster, Austria) were used. Blood was transported to a laboratory located in the room next to the one in which the blood sampling took place to prepare the plasma, diluted plasma, and diluted blood.

### 2.5. Preparation of Human Plasma and Blood

A total of 100  $\mu$ L of the trisodium citrate blood was removed and placed into an Eppendorf tube. The rest of the sample was centrifuged to obtain plasma. To sediment the erythrocytes, blood was centrifuged at room temperature for 10 min at  $1480\times g$  (centrifuge Centric 322A, Domel, Železniki, Slovenia). The supernatant from above the buffy coat was collected in an Eppendorf tube to constitute a 200  $\mu$ L plasma aliquot. The same procedure was used for the preparation of the potassium EDTA samples. Blood and plasma samples were transported to the laboratory (by bicycle (ca. 1 km)) where the measurements by means of ILM took place.

### 2.6. Preparation of Diluted Canine Plasma and Blood

A total of 5  $\mu$ L of EDTA whole blood was pipetted into 995  $\mu$ L of saline ( $200\times$  dilution). The rest of the EDTA whole blood was centrifuged to obtain plasma; to sediment the erythrocytes, the blood was centrifuged for 15 min at  $1500\times g$  and  $21\text{ }^{\circ}\text{C}$  (centrifuge Heraeus Megafuge 8R, Thermo Fisher Scientific, Osterode Am Harz, Germany). The supernatant from above the buffy coat was collected into Eppendorf tubes to constitute 250  $\mu$ L plasma aliquots. A total of 4  $\mu$ L of EDTA plasma was pipetted into 196  $\mu$ L of saline ( $50\times$  dilution). Plasma, diluted plasma, and diluted blood samples were transported to the laboratory (by car (ca. 1 km)) where the measurements by means of ILM took place.

### 2.7. Interferometric Light Microscopy (ILM)

Samples were processed within 4 h from the sampling. The average  $n$  and  $D_h$  of the EPs were determined by means of ILM using Videodrop (Myriade, Paris, France). If convenient, samples were additionally diluted with physiologic saline (B. Braun Melsungen AG, Melsungen, Germany) that was kept in sealed containers at room temperature—to reach the optimal number density of EPs for detection (between  $5\times 10^8$  and  $5\times 10^9$  particles per mL in the sample). Measurements were performed at room temperature. The signals of the saline were under the detection limit. A total of 7  $\mu$ L of sample was placed between cover glasses and illuminated by a 2 W blue LED light. A threshold value of 4.2 was used. The light shed on the sample and the light scattered on the particles was imaged using a bright-field microscope objective. Images of the interference between the incident and scattered light were captured using a complementary metal–oxide–semiconductor high-resolution, high-speed camera and analyzed. The signal of the incident light was subtracted from the image. Patterns that included contrasting black and white spots were recognized as particles. The number density of the particles was estimated as the ratio between the number of detected particles and the volume scanned (e.g., 15 pL). The movement of every particle was recorded on video. The  $D_h$  of a particle was determined by tracking the position of the imaged particle in the recorded video. Each video consisted of 100 frames recorded at 140 frames per second (lasting less than one second). Several successive videos

were made, and the time that elapsed between two videos was about 15 s. It is estimated that about 90% of the nanoparticles undergoing Brownian motion in a typical volume imaged by ILM move out of that volume in about 0.45 s. Consequently, the nanoparticle population is almost completely renewed in each video. If a nanoparticle was detected in a different frame within the video, its track was reconstructed. The diffusion coefficient ( $D$ ) of the motion of the particle was taken proportional to the mean square displacement ( $d$ ) of the particle between two consecutive recorded frames taken in the time interval  $\Delta t$ ,  $\langle d^2(\Delta t) \rangle = \langle 4D \Delta t \rangle$  (where the parentheses  $\langle \rangle$  mark the averaging). The  $D_h$  value was estimated by assuming that the particles were spherical and using the Stokes–Einstein relation  $D_h = kT/3\pi\eta D$ . A limit of 10 movies or 300 detected particles was set for each sample. Processing of the images and of the movies was performed using the associated software QVIR 2.6.0 (Myriade, Paris, France).

### 2.8. Scanning Electron Microscopy of Plasma (SEM)

A total of 20 microliters of sample was placed on a 50 nm carbon filter in the incubation chamber, and 40 microliters of 1% OsO<sub>4</sub> solution was poured on top. After incubation for 1 h, the solution was pushed through the filter. The filter was removed from the incubation chamber and placed in a well filled with distilled water. The filter was incubated in water for 10 min, repeated 3 times. Then, the filter was dehydrated in a graded series of ethanol (30%, 50%, 70%, 80%, 90%, and 100%, 10 min each) and hexamethyldisilazane mixed with absolute ethanol (30%, 50%, and 100%, 10 min each) and, finally, air-dried. The dried sample was sputtered with a mixture of gold and palladium and examined with a scanning electron microscope (JSM-6500F, JEOL Ltd., Tokyo, Japan).

### 2.9. Cryogenic Transmission Electron Microscopy (cryoTEM)

Aliquots of 250  $\mu$ L of plasma were placed in Eppendorf tubes and centrifuged for 10 min at  $17,570 \times g$  and at room temperature in a Centric 200R centrifuge with a Lilliput rotor (Domel, Železniki, Slovenia). The upper 200  $\mu$ L of supernatant was replaced with saline, resuspended, and centrifuged again for 10 min at  $17,570 \times g$  and room temperature in the Centric 200R centrifuge with Lilliput rotor (Domel, Železniki, Slovenia). A total of 200  $\mu$ L of supernatant was removed, and the pellet gathered from the aliquots was suspended in 80  $\mu$ L of saline for imaging with CryoTEM Vitrobot Mark IV (Thermo Fisher Scientific, Waltham, MA, USA). The C-flat (2  $\mu$ m hole size, 2  $\mu$ m hole spacing, 200 mesh holey carbon grids (EMS, Hatfield, PA, USA)) were glow discharged for 60 s at 20 mA and positive polarity in an air atmosphere (GloQube<sup>®</sup> Plus, Quorum, Laughton, UK). The conditions were set at 4 °C, 95% relative humidity, blot time: 7 s, and blot force: 2. Three  $\mu$ L of the sample with nanoparticles in suspension was applied to the grid, blotted, and vitrified in liquid ethane. Samples were visualized under cryogenic conditions using a 200 kV Glacios microscope with a Falcon 3EC detector (Thermo Fisher Scientific, Waltham, MA, USA).

### 2.10. Statistical Analysis

All measurements were performed in triplicate and are presented as the average value and standard deviations. The number of samples included in the final analysis was lower than the number of samples acquired, as for some samples, the number density of EPs was under the detection limit or technical issues occurred in their transport and handling. The number of samples included in the assessment of each parameter is provided with the results. Correlations between variables were assessed using the Pearson correlation coefficient ( $r$ ) and the respective probability ( $p$ ). A value of  $p = 0.05$  was taken as the threshold for statistical significance. Differences between samples were determined by the  $t$ -test and respective probability ( $p$ ), with a value of  $p = 0.05$  taken as the threshold for statistical significance. For statistically significant differences, statistical power was calculated using Web-based Sample Size/Power Calculations; Inference for Means: Comparing Two

Independent Samples <https://www.stat.ubc.ca/~rollin/stats/ssize/n2.html> (accessed on 28 October 2024). The value of statistical power  $P > 0.8$  was taken as sufficient.

### 3. Results

The raw data used to compose Figures 1 and 2, as well as Tables 1–4, are provided in the Supplementary Materials. Figure 1 shows the interdependencies between  $n$  (corrected for dilution) and  $D_h$  in human plasma, human blood, canine plasma, and canine blood. In human samples, two anticoagulants were considered (trisodium citrate and EDTA). It can be seen that at higher values of  $n$ , the  $D_h(n)$  dependence saturated to an expected constant value; however, it increased considerably with a decrease in  $n$  (Figure 1a–c). This was observed for all groups of samples, but it was more notable for plasma than blood (Figure 1a and black circles in Figure 1c). The measurements in blood exhibited higher scattering over the whole range of  $n$  (Figure 1b and empty circles in Figure 1c) which masked the effect.

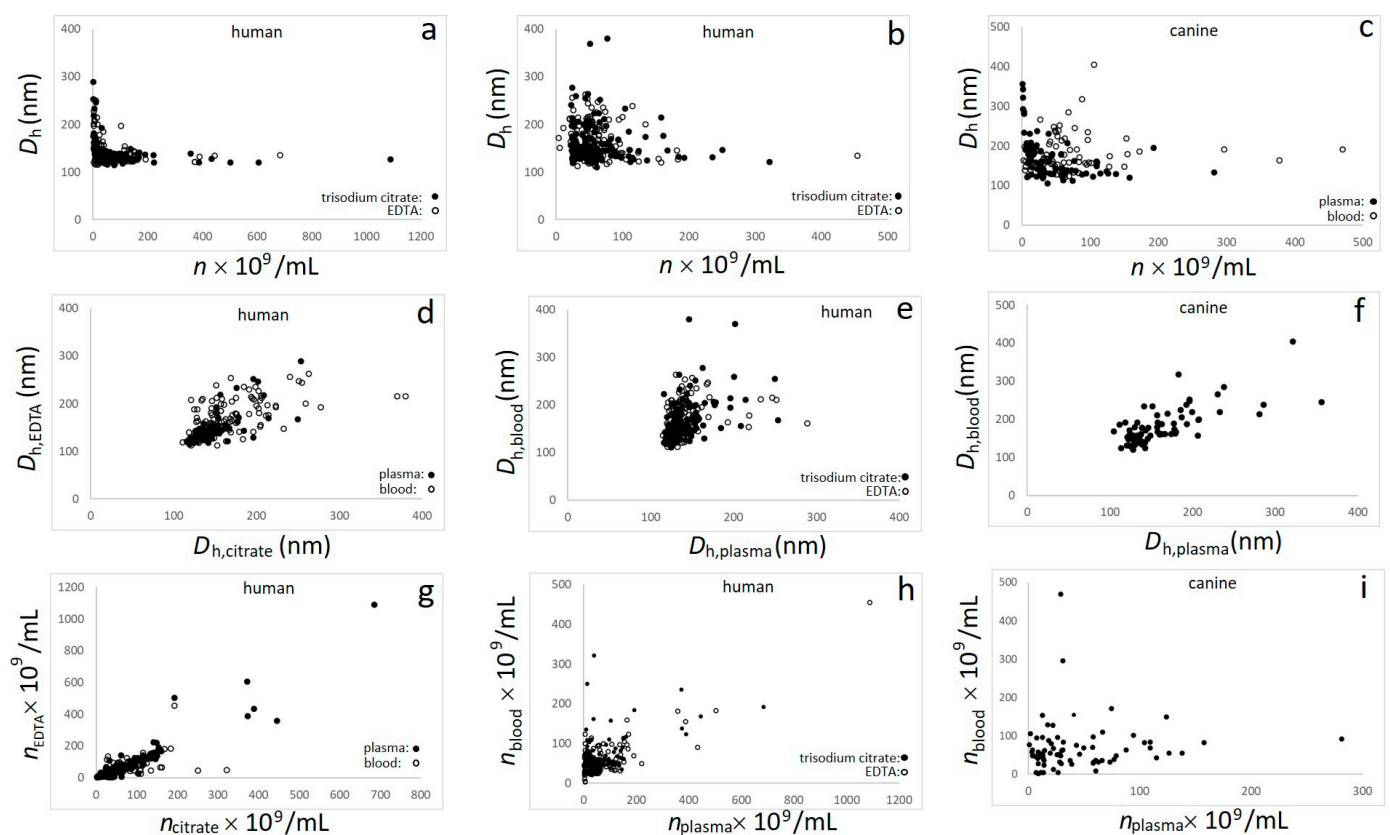


**Figure 1.** (a) Hydrodynamic diameter of EPs  $D_h$  as a function of the number density of EPs  $n$  in human plasma; (b)  $D_h$  as a function of  $n$  in human blood; (c)  $D_h$  as a function of  $n$  in canine plasma and blood; (d) agreement between  $D_h$  of EPs in the samples collected in two anticoagulants (trisodium citrate and EDTA); (e) agreement between  $D_h$  of EPs in human plasma and in human blood; (f) agreement between  $D_h$  of EPs in canine plasma and in canine blood; (g) agreement between  $n$  in samples collected in two anticoagulants (trisodium citrate and EDTA); (h) agreement between  $n$  in human plasma and in human blood; (i) agreement between  $n$  in canine plasma and in canine blood.

The correlations between the assessed  $D_h$  in the human plasma with trisodium citrate and  $D_h$  in the human plasma with EDTA, as well as between  $n$  in the human plasma with trisodium citrate and  $n$  in the human plasma with EDTA, were strong and the dependencies exhibited the expected 1:1 slope (Figure 1d,g), suggesting that at the population level the choice of the anticoagulant did not have a detectable effect on the results. The  $D_h$  in human plasma and  $D_h$  in human and canine blood were strongly correlated; however, the slopes

indicated larger EPs in blood than in plasma (Figure 1e,f). We found a statistically highly significant correlation between  $n$  in plasma and in blood in human (Figure 1h) but not in the dog (Figure 1i).

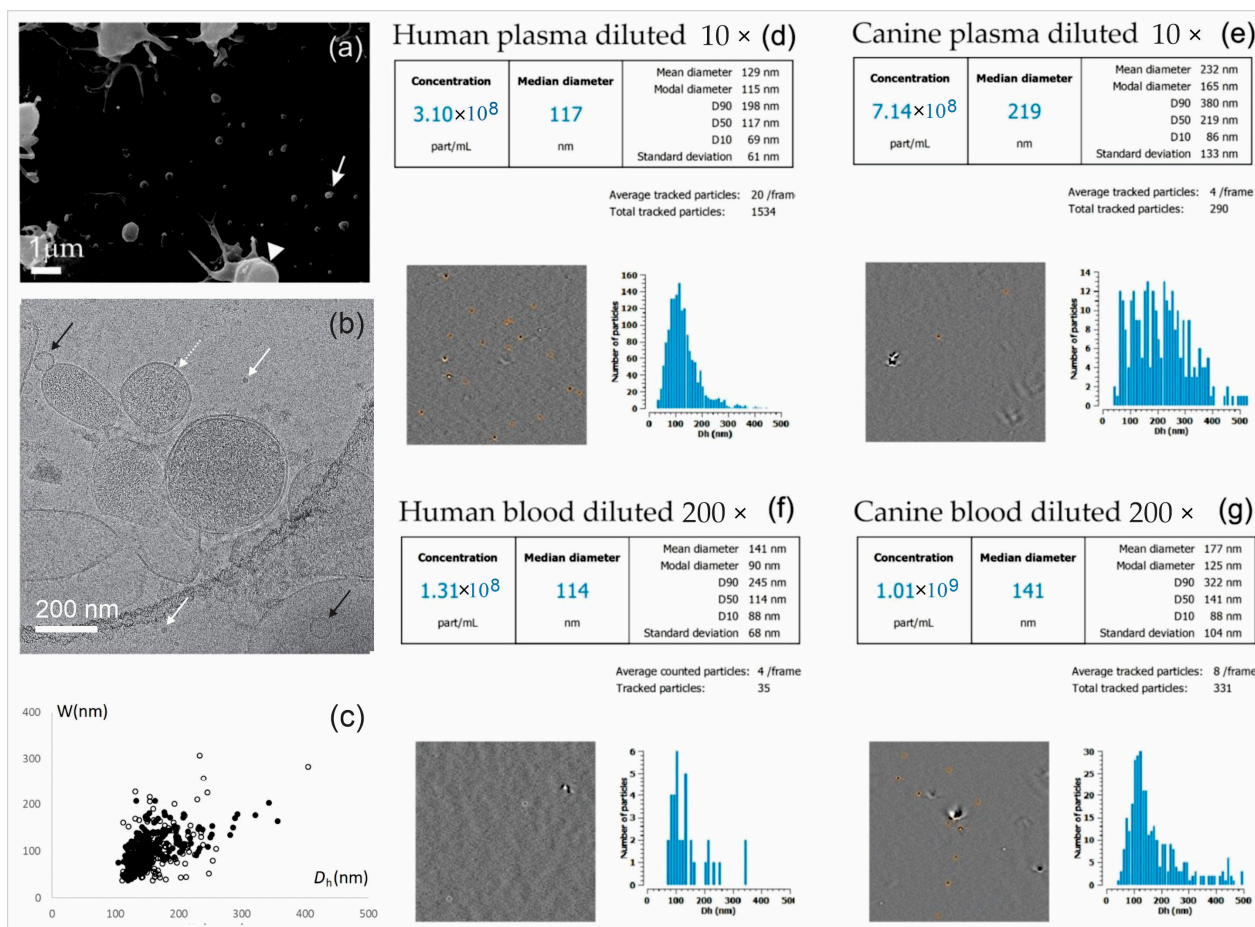


**Figure 2.** (a) Scanning electron micrograph of the canine plasma showing EPs (white arrow) and platelets (white triangle); (b) cryogenic transmission electron micrograph of EPs isolated from human plasma showing membrane-enclosed vesicles of various sizes (dashed white arrow points to a large vesicle, and black arrows point to smaller vesicles) and molecular complexes (white arrows); (c) correlation between  $D_h$  and the width of the distribution  $W$  for all analyzed samples (full circles: plasma; empty circles: blood); (d–g) examples of ILM results of human plasma and blood and of canine plasma and blood showing the distribution over  $D_h$  and displaying the detected particles (orange circles).

The Pearson coefficients of the various correlations are presented in Table 1. It can be seen that all correlations, but correlation between  $n$  in the canine plasma and  $n$  in the canine blood, were highly statistically significant ( $p < 10^{-4}$ ). The strongest correlations were found for the human plasma between the two anticoagulants in  $n$  ( $r = 0.94$ ; Table 1 and Figure 1g) and  $D_h$  ( $r = 0.77$ ; Table 1 and Figure 1d), as well as between  $n$  in human plasma and blood with EDTA anticoagulant ( $r = 0.81$ ; Table 1 and Figure 1h). It can be seen that the Pearson coefficients could reach values higher than 0.9, which sets a high standard for the achievable level of quality for assessments via ILM.

We considered (see Section 4: Discussion) that the steep increase in  $D_h$  with a decrease in  $n$  at low  $n$  is partly an artifact. In a further statistical analysis, we therefore placed confidence in the results for the region of  $n$  where  $D_h$  had saturated and assumed that the  $D_h$  values of a great majority of EPs in vivo are smaller than 250 nm. Because of the above

arguments regarding the quality of the measurements (Figure 1a–c), we discarded samples with  $D_h$  larger than 250 nm in estimation of the population averages  $\langle n \rangle$  and  $\langle D_h \rangle$ .

**Table 1.** Pearson correlation coefficients between  $D_h$  of EPs in human plasma and human blood;  $n$  of EPs in human plasma and human blood, collected in tubes with two different anticoagulants: trisodium citrate and EDTA, between  $D_h$  in plasma and blood, and between  $n$  in plasma and blood, in human and canine samples.

Human	$D_{h,citrate,plasma}$	$D_{h,EDTA,plasma}$	$D_{h,citrate,blood}$	$D_{h,EDTA,blood}$
$D_{h,citrate, plasma}$	1	0.77 ( $p < 10^{-5}$ , $N = 151$ ) *	0.48 ( $p < 10^{-5}$ , $N = 149$ ) *	0.41 ( $p < 10^{-5}$ , $N = 146$ ) *
$D_{h,EDTA, plasma}$		1	0.39 ( $p < 10^{-5}$ , $N = 148$ ) *	0.34 ( $p = 3 \times 10^{-5}$ , $N = 145$ ) *
$D_{h,citrate, blood}$			1	0.61 ( $p < 10^{-5}$ , $N = 143$ ) *
$D_{h,EDTA, blood}$				1
	$n_{citrate,plasma}$	$n_{EDTA,plasma}$	$n_{citrate,blood}$	$n_{EDTA,blood}$
$n_{citrate, plasma}$	1	0.94 ( $p < 10^{-5}$ , $N = 150$ ) *	0.49 ( $p < 10^{-5}$ , $N = 148$ ) *	0.73 ( $p < 10^{-5}$ , $N = 146$ ) *
$n_{EDTA, plasma}$		1	0.49 ( $p < 10^{-5}$ , $N = 146$ ) *	0.81 ( $p < 10^{-5}$ , $N = 144$ ) *
$n_{citrate, blood}$			1	0.47 ( $p < 10^{-5}$ , $N = 142$ ) *
$n_{EDTA, blood}$				1
Human, Canine	$D_{h,human plasma}$	$D_{h,canine plasma}$	$n_{human plasma}$	$n_{canine plasma}$
$D_{h,human blood}$	0.41 ( $p < 10^{-5}$ , $N = 294$ ) *			
$D_{h,canine blood}$		0.72 ( $p < 10^{-5}$ , $N = 76$ ) *		
$n_{human blood}$			0.66 ( $p < 10^{-5}$ , $N = 292$ ) *	
$n_{canine blood}$				0.07 ( $p = 0.55$ , $N = 76$ )

Probability indicating the statistical significance of the correlation ( $p$ ) and the number of samples included for each correlation ( $N$ ) considered. Asterisks denote statistically significant correlations of  $p < 0.05$ .

**Table 2.** Average hydrodynamic diameter  $\langle D_h \rangle$  of EPs in human and canine plasma and in human and canine blood, the difference in the respective  $\langle D_h \rangle$ , and the corresponding probability of statistical significance ( $p$ ) and statistical power ( $P$ ) (in cases with  $p < 0.05$ ). Human blood was collected in tubes with two different anticoagulants, trisodium citrate and EDTA; canine blood was collected in EDTA.

Sample	$\langle D_{h,citrate} \rangle \pm SD$ (nm)	$\langle D_{h,EDTA} \rangle \pm SD$ (nm)	Difference (%)	p/P
Human plasma	140 ± 4 (N = 165)	137 ± 4 (N = 149)	−2	0.519
Human blood	155 ± 9 (N = 142)	162 ± 11 (N = 143)	4	0.645
Difference (%)	10	17		
p/P	$<10^{-5}/1$ *	$<10^{-5}/1$ *		
	$\langle D_{h,plasma} \rangle \pm SD$ (nm)	$\langle D_{h,blood} \rangle \pm SD$ (nm)		
Human	139 ± 31 (N = 315)	158 ± 11 (N = 285)	13	$<10^{-5}/1$ *
Canine	155 ± 32 (N = 81)	171 ± 33 (N = 71)	10	0.003/0.82
Difference (%)	11	8		
p/P	$<10^{-5}/1$ *	0.002/0.65		

The difference between any b and a was calculated as  $2 \times (b - a)/(a + b)$ . N = the number of samples in the population. Asterisks mark statistically significant differences ( $p < 0.05$ ) that have sufficient statistical power ( $P > 0.8$ ).

The  $\langle D_h \rangle$  values in the samples with trisodium citrate did not differ from the  $\langle D_h \rangle$  values in the samples with EDTA both in the plasma and blood (Table 2). In both the human and canine samples,  $\langle D_h \rangle$  in blood was higher than that in plasma (Table 2). The  $\langle D_h \rangle$  value in the canine samples was higher than that in the human samples, for both plasma and blood (Table 2). All statistically significant differences, but the difference between the canine plasma and canine blood, were of sufficient statistical power ( $P \geq 0.8$ ).

The average number densities  $\langle n \rangle$  of EPs in human plasma with trisodium citrate and with EDTA, in human blood with trisodium citrate and with EDTA, and in human blood and plasma with trisodium citrate showed no statistically significant differences (Table 3). The difference between  $\langle n \rangle$  in the canine plasma and blood was statistically significant with sufficient statistical power (Table 3).



**Table 3.** Average number density  $\langle n \rangle$  of EPs in human and canine plasma and in human and canine blood, the difference in the respective  $\langle n \rangle$ , the corresponding probability of statistical significance (p), and statistical power (P) (in cases with  $p < 0.05$ ). Number densities are corrected for the dilution of samples. Human blood was collected in tubes with two different anticoagulants, trisodium citrate and EDTA; canine blood was collected in EDTA.

Sample	$\langle n_{\text{citrate}} \rangle \pm \text{SD} \times 10^9/\text{mL}$	$\langle n_{\text{EDTA}} \rangle \pm \text{SD} \times 10^9/\text{mL}$	Difference (%)	p/P
Human plasma	60.7 ± 65.2 (N = 165)	71.7 ± 152.5 (N = 149)	17	0.053
Human blood	63.2 ± 53.4 (N = 141)	58.8 ± 56.4 (N = 143)	−7	0.167
Difference (%) & p/P	4 0.759	−20 0.239		
	$\langle n_{\text{plasma}} \rangle \pm \text{SD} \times 10^9/\text{mL}$	$\langle n_{\text{blood}} \rangle \pm \text{SD} \times 10^9/\text{mL}$		
Human	65.4 ± 154.9 (N = 314)	61.0 ± 49.4 (N = 285)	−7	0.461
Canine	46.8 ± 46.7 (N = 81)	73.7 ± 76.2 (N = 71)	45	0.009/0.8
Difference (%) p/P	−33 0.11	22 0.07		

& The difference between a and b was calculated as  $2 \times (a - b)/(a + b)$ . N = the number of samples in the population.

**Table 4.** Average measured (uncorrected for dilution) number density  $\langle n \rangle$  of EPs in human plasma and in human blood collected in tubes with two different anticoagulants, trisodium citrate and EDTA and in canine plasma and canine blood, with the respective average dilution of the sample and number of particles measured ( $N_{\text{tracked}}$ ).

Sample	$\langle n_{\text{citrate}} \rangle \pm \text{SD} \times 10^9/\text{mL}$	$\langle \text{Dilution}_{\text{citrate}} \rangle$	$N_{\text{tracked}}$	$\langle n_{\text{EDTA}} \rangle \pm \text{SD} \times 10^9/\text{mL}$	$\langle \text{Dilution}_{\text{EDTA}} \rangle$	$N_{\text{tracked}}$
Human plasma	1.30 ± 0.84 (N = 163)	41 ± 53	114,772	1.31 ± 0.84 (N = 149)	46 ± 76	108,383
Human blood	0.22 ± 0.19 (N = 141)	302 ± 118	19,828	0.22 ± 0.28 (N = 142)	315 ± 116	18,375
Canine plasma				1.29 ± 1.18 (N = 81)	37 ± 25	48,998
Canine blood				0.30 ± 0.53 (N = 71)	348 ± 236	11,659

N = the number of samples in the population.

The recommended optimal range for the measured  $n$  of the ILM equipment was between  $0.5 \times 10^9/\text{mL}$  and  $5.0 \times 10^9/\text{mL}$ . Most plasma samples were within this interval ( $\langle n \rangle$  (uncorrected for dilution) in human plasma was  $1.30 \times 10^9/\text{mL}$  in trisodium citrate, and  $1.31 \times 10^9/\text{mL}$  in EDTA and in canine samples it was  $1.29 \times 10^9/\text{mL}$  (Table 4)). In blood, the measured values of  $\langle n \rangle$  were considerably smaller ( $0.22 \times 10^9/\text{mL}$  in both trisodium citrate and EDTA in human samples, as well as  $0.30 \times 10^9/\text{mL}$  in canine samples) (Table 4), which is out of the recommended optimal range, but still notably higher than the signal of the saline which was always lower than  $0.1 \times 10^9/\text{mL}$ . The blood samples were more diluted to enable saturation of light which was expected to be absorbed in the residual cells. The range of dissipation of the number densities ( $n$ ) in the blood samples was larger in blood than in plasma (Figure 1a–c), which is reflected in the respective standard deviations that are comparable to the average values (Tables 3 and 4).

In ILM, each particle is tracked by recording a video and analyzed individually. It follows from Table 4 that more than 270,000 EPs have been assessed in human samples and more than 70,000 in canine samples.

Figure 2 shows a SEM image of canine plasma and a cryoTEM image of EPs isolated from human plasma. For the cryoTEM, the cells had to be removed from the sample by means of filtering. Figure 2a shows EPs (white arrow) and residual activated platelets (white triangle) with tubular protrusions. EPs are globular and heterogeneous in size. Figure 2b shows membrane-enclosed particles of different sizes, in agreement with Figure 2a. The width of the distribution over  $D_h$  for each sample is represented by the standard deviation of the distribution ( $W$ ). Figure 2c shows the correlation between  $D_h$  and  $W$  for all analyzed samples. The Pearson correlation coefficient is 0.63 in plasma and 0.48 in blood; both correlations are highly statistically significant ( $p < 10^{-5}$ ). Examples of the distributions are presented in Figure 2d–g. In the human plasma and blood examples (Figures 2d and 2f, respectively),  $D_h$  is small and the distribution is narrow (i.e., the reported standard deviation

is small). In the canine examples, the distributions are wider, and the average values of  $D_h$  are higher (Figure 2e,g). In the interference micrographs, identified EPs are marked with orange circles. The presence of singular, larger particles can be noted.

## 4. Discussion

### 4.1. Need of Sufficient Population Size for Translational Medicine

EPs derived from blood are of the utmost interest for diagnostics, monitoring, and therapeutics, as they may travel via circulation and reach areas that are not directly accessible in an intact body. Since Wolf (1967) indicated their important biological role [1], EPs have been the subject of extensive study [2–4]. However, in spite of their potential involvement in basic cellular processes and the vast amount of accumulated data, to the best of our knowledge, methods based on blood-derived EPs have not yet made a breakthrough into everyday clinical practice. This proves that translation of basic EV research into clinical practice is a challenging task [5,39].

In analyses of small populations, it is questionable whether the cases are representative and whether the results are based on differences between the populations or on the noise caused by the limitations of the methods. Clinical studies involving EPs are often limited by a relatively small number of cases reflecting lengthy and/or sophisticated harvesting procedures, too small a yield of EPs—even to apply multiple assessment techniques—and insufficient repeatability of the procedures. A meta-analysis that included 716 comparisons between populations of EP samples [46] reported that 308 (43%) comparisons had statistically significant differences ( $p < 0.05$ ). Sufficient statistical power ( $P > 0.8$ ) was found in 242 (34%) and clinical significance, estimated as a modified Reliable Change Index larger than 1.96 (less than 5% false-positive and/or false-negative results) [46], was found only in 88 (12%). None of the studies amid the 12% included more than 50 cases within both populations [46]. Pursuing decisive answers regarding clinically relevant questions must be based on methods that enable the analysis of sufficiently large populations of samples. Our results prove that analysis of diluted blood and diluted plasma with ILM enables the determination of basic information (number density and size of EPs and their hydrodynamic diameter) in large cohorts of samples.

### 4.2. Less Is More in Sample Processing

To obtain plasma, erythrocytes are removed, and this is usually performed by centrifugation of blood. The movement of blood cells during centrifugation is rather complex and may be a source of EV shedding (particularly from platelets) [47]. Platelets are prone to fragment because of shear stress which develops during sampling and centrifugation [37,48,49]. In principle, to minimize platelet activation and fragmentation, sampling of blood should be as gentle as possible regarding the shear stress; shaking of samples (e.g., during transport) should be avoided, and it would be best to process the samples immediately at the same location where the blood was sampled.

It was recently reported [47] that during erythrocyte sedimentation, plasma is pushed in the opposite direction, thereby carrying platelets, EPs, and molecules toward the top of the tube. In this phase, the supernatant becomes enriched in platelets and small particles. However, when the lower bound of the plasma meets with the upper bound of the erythrocytes, further centrifugation sediments also the platelets and, to a certain extent, the EPs, so plasma becomes poorer with these constituents [47]. The process depends on the physical properties of the blood and on the geometry of the tubes and centrifuge rotor. The shear forces acting on the platelets depend on the viscosity of the medium, which is in turn sensitive to the temperature. Taking blood out of the body exerts thermic stress on the cells [36]. Centrifugation of blood is usually performed in refrigerated centrifuges that have a feedback loop to level the temperature in the rotor chamber by turning on the cooling when the temperature, which increased because of the friction of the bearings, exceeds the required value. The timing of this occurrence is not repeatable and may strike the samples in different particle distribution configurations. Usually, plasma is prepared using the same

centrifuge settings for all samples, although the properties of the samples are different and are affected by the same external parameters to a different degree. On the other hand, with respect to the randomness of the processing parameters described above, it would be best if the blood samples were centrifuged within the same lot. However, the number of samples that can be loaded into the centrifuge is rather small, and even with this number, some samples must wait. During isolation/enrichment and assessment procedures, particles in plasma are exposed to further mechanical stress or physicochemical modifications, which does not affect all samples evenly, as they have different compositions and physical properties. All of the above processes may differ considerably among individual samples.

It was reported that the presence of small amounts of particles up to 1  $\mu\text{m}$  in size generally does not compromise the accuracy of the NTA measurements [50]. In DLS, the intensity of the scattered light is proportional to the square of the volume of the particle, which makes DLS very sensitive to the presence of large particles; small amounts of large aggregates or dust particles can disturb the size determination if the main population is significantly smaller in size [51]. Therefore, larger particles (e.g., cells) should be removed from the samples prior to the measurement. In isolation and characterization, the noise increases with each step. Omitting procedures in processing means the only possibility of avoiding certain sources of artefacts.

#### 4.3. Characterization of Human IBD and Canine BOAS Populations

The principal aim of the IBD and BOAS clinical studies (albeit beyond the scope of this work) was to see whether EPs can be used as a parameter to follow-up on the effect of the treatment. The BOAS study was the first to start. The Small Animal Clinic at the Veterinary Faculty, University of Ljubljana, has skilled technicians and a well-equipped laboratory next door to the room where the blood sampling is performed. This was particularly advantageous, as previous work indicated the importance of avoiding any stress in transporting and saving the samples [37]. The staff had experience in blood sampling for EP assessment from a previous collaboration. Therefore, it seemed optimal to process the samples immediately after the sampling at the clinics. A small amount of blood was diluted and the rest was centrifuged to obtain plasma. As we did not have experience, we did not know what would be appropriate range of the dilution. The dilutions of plasma ( $50\times$ ) and blood ( $200\times$ ) were set based on previous results [47]. Moreover, the rest of the plasma was conserved to allow for different dilutions. These samples were transported by car to the laboratory for measurement with ILM (distance of about 1 km) and were assessed within 4 h of the sampling. On the other hand, the sampling of blood from patients with IBD took place at the University Medical Centre, Ljubljana. Samples were transported to the Faculty of Pharmacy (ca. 3 km away) by bicycle. A part of the blood was saved and another part centrifuged to produce plasma. Undiluted blood and plasma were transported by bicycle to the laboratory where appropriate dilutions of blood and plasma and measurement with ILM took place (distance of about 1 km). Although the design of the study and laboratory configuration was more favorable in the BOAS study, strong correlations were found between all parameters, except between  $n$  in canine plasma and blood (Table 1). It seems that the decisive difference between the two studies is in the dilution of the blood samples. In canine blood, the results fell within the range of a low  $n$ /large  $D_h$  region of  $D_h(n)$  dependence that is subject to artefacts and large dissipation of the results (Figure 1c). Too high dilution and a uniform choice of dilution for all samples in the BOAS study turned out to be a disadvantage over the possibility to adjust the dilution to the individual sample (which took place in the IBD study). The sampling design, preparation of plasma, and dilution and transport of samples should be further improved also considering the individualization of plasma and blood preparation. However, the results derived from the parallel cohorts of samples were valuable, as such experiences point to possible limitations and accelerate the optimization of the methods. An evaluation of the correlation between EPs in plasma and blood is plausible and feasible, and it could be considered for use in assessing the quality of the processing.

4.4. Comparison with Studies in the Literature

Table 5 presents  $\langle n \rangle$  and  $\langle D_h \rangle$  of EPs obtained in this study with  $\langle n \rangle$  and size estimations from studies found in the literature. We performed a search according to keywords (e.g., plasma, blood, extracellular vesicles, extracellular particles, size, and concentration) in Google Scholar. We present a comparison of our results with 55 cohorts of EP samples (30 studies) using different preparations of plasma and different assessment techniques. We found two studies considering assessment of EPs directly in diluted blood by FCM [38,39]. Comparing  $\langle n \rangle$  of EPs in diluted blood shows that the results obtained by FCM were four orders of magnitude smaller than our results (obtained by ILM), despite the sample preparation methods being similar (dilution of blood in PBS [39] or saline (this work)).

**Table 5.** Estimation of the size and number density of EPs in the selected studies.

Reference	Cohort	Method of Harvesting	Method of Assessment	N	Average Size (nm)	Average Number Density $\times 10^9$ /mL
<b>Blood</b>						
This work	IBD	fresh, dilution	ILM	296	158 $\pm$ 11	61 $\pm$ 48
This work	canine BOAS	fresh, dilution	ILM	71	171 $\pm$ 33	75 $\pm$ 83
Marchisio et al., 2021 [37]	healthy	fresh, dilution	FCM	22	>160 nm	0.0083 $\pm$ 0.0042
Brocco et al., 2022 [38]	pancreatic cancer	fresh, dilution	FCM	56		0.0021
Brocco et al., 2022 [38]	healthy	fresh, dilution	FCM	48		0.0016
<b>Plasma</b>						
This work	IBD	fresh, dilution	ILM	303	136 $\pm$ 31	68 $\pm$ 106
This work	canine BOAS	fresh, dilution	ILM	81	155 $\pm$ 32	49 $\pm$ 48
Berry et al., 2024 [44]	multispecies	fresh, dilution	ILM	250	130–200	
Kogej et al., 2021 [23]	ovarian cancer	fresh, dilution	DLS	7	20–40	
Mork et al., 2016 [41]	healthy	fresh, dilution	NTA	20	42–73	89–1000
Mork et al., 2016 [41]	healthy	fresh, dilution	TRPS	20	171–276	0.21–1.30
de Vrij et al., 2013 [42]	healthy	fresh, dilution	TRPS	NS	$\approx$ 200	0.2
Gardiner et al., 2013 [35]	NS	NS	NTA	NS		1000–5000
Holcar et al., 2024 [52]	healthy	thawed	FCM	208		0.0002–0.042
Botha et al., 2021 [43]	NS	thawed	FCM	NS		$\approx$ 0.0008
Robinson et al., 2024 [40]	healthy	thawed	NTA	3	$\approx$ (65–80)	987
Lawrie et al., 2009 [20]	healthy	thawed	DLS	20	77–266	
<b>Isolated EVs</b>						
Gardiner et al., 2013 [35]	NS	UC	NTA	NS	70–120	5–50
Elgamal et al., 2021 [53]	NS	UC	NTA	44		219 $\pm$ 9.5
Osti et al., 2019 [54]	glioblastoma preop.	UC	NTA	13	95 $\pm$ 20	69.7 $\pm$ 9.7
Osti et al., 2019 [54]	healthy	UC	NTA	17	100 $\pm$ 15	21.2 $\pm$ 2.8
Osti et al., 2019 [54]	glioblastoma postop.	UC	NTA	30	120 $\pm$ 12	34.5 $\pm$ 3.8
Osti et al., 2019 [54]	healthy	UC	NTA	16	128 $\pm$ 20	19.6 $\pm$ 2.2
Bettio et al., 2023 [55]	healthy	UC	NTA	30	153	17.8
Jamaly et al., 2018 [56]	healthy	UC	NTA	10	$\approx$ (70–90)	$\approx$ (20–25)
Serrano-Pertierra et al., 2019 [57]	healthy	UC	DLS	3	152.09 $\pm$ 29.38	
Serrano-Pertierra et al., 2019 [57]	healthy	UC	NTA	3	208.5 $\pm$ 10.60	603
Malys et al., 2021 [58]	healthy	UC	NTA	9	148.11 $\pm$ 14.64	0.27 $\pm$ 0.22
George et al., 2021 [59]	NS	UC	NTA	NS	150	400 $\pm$ 170
Holcar et al., 2024 [52]	healthy	UC	NTA	208	152	5.7
Scavo et al., 2019 [60]	healthy	UC	DLS	8	132	
Scavo et al., 2019 [60]	colorectal cancer	UC	DLS	22	151	
Scavo et al., 2019 [60]	gastric cancer	UC	DLS	8	157	
Dlugolecka et al., 2021 [61]	lung cancer	UC	NTA	34	98.43 $\pm$ 10.31	244 $\pm$ 471
Picciolini et al., 2021 [62]	healthy	SEC	NTA	10	167 $\pm$ 9.4	23.4
Picciolini et al., 2021 [62]	Alzheimer’s disease	SEC	NTA	10	183 $\pm$ 4.6	118
Contreras et al., 2023 [63]	healthy	SEC	NTA	3	119.4 $\pm$ 6.9	
Stranska et al., 2018 [64]	healthy	SEC	NTA	6	117	10
Diehl et al., 2023 [65]	healthy	SEC	TRPS	12	77.75	60
Diehl et al., 2023 [65]	Marfan syndrome	SEC	TRPS	6	69.92	147
Franco et al., 2023 [66]	healthy, idiopathic inflammatory myopathy	SEC, UF	NTA	70	202 $\pm$ 19	15.1 $\pm$ 10.6
Malys et al., 2021 [58]	healthy	SEC	NTA	9	132.52 $\pm$ 12.05	4975.6 $\pm$ 769.5

Table 5. Cont.

Serrano-Pertierra et al., 2019 [57]	healthy	precipitation	DLS	3	76.64 ± 16.17	
Serrano-Pertierra et al., 2019 [57]	healthy	precipitation	NTA	3	203.67 ± 55.41	1263
Longobardi et al., 2021 [67]	Alzheimer’s frontotemporal dementia	precipitation	NTA	30	133.8 ± 17.1	147 ± 61.8
Longobardi et al., 2021 [67]	dementia with Lewy bodies	precipitation	NTA	30	130.2 ± 18.8	139 ± 61
Longobardi et al., 2021 [67]	healthy	precipitation	NTA	30	113 ± 13.2	249 ± 118
Serrano-Pertierra et al., 2019 [57]	healthy	precipitation	DLS	3	123.55 ± 63.04	
Serrano-Pertierra et al., 2019 [57]	healthy	precipitation	NTA	3	233.97 ± 33.73	7383
König et al., 2017 [68]	breast cancer	precipitation	NTA	105	140	≈2500
König et al., 2017 [68]	healthy myalgic encephalomyelitis/chronic fatigue syndrome	precipitation	NTA	16		≈60
Giloteux et al., 2020 [69]	healthy	precipitation	NTA	35	130.1 ± 12.7	7.6 ± 5.0
Giloteux et al., 2020 [69]	healthy	precipitation	NTA	35	132.7 ± 16.4	6.6 ± 4.3
Stranska et al., 2018 [64]	healthy	membrane-based affinity binding	NTA	6	210	40
Bettio et al., 2023 [55]	healthy	membrane-based affinity binding	NTA	30	238	23.2
Scavo et al., 2019 [60]	healthy	UC	TEM	8	87	
Scavo et al., 2019 [60]	colorectal cancer	UC	TEM	22	108	
Scavo et al., 2019 [60]	gastric cancer	UC	TEM	8	112	

N: number of cases; NS: nonspecified; UF: ultrafiltration.

In the assessment of  $\langle n \rangle$  directly in diluted plasma, the values spanned seven orders of magnitude—between  $2 \times 10^5$ /mL (FCM [52]) and  $5 \times 10^{12}$ /mL (NTA [35]). Isolation by UC yielded  $\langle n \rangle$  between  $0.27 \times 10^9$ /mL [58] and  $603 \times 10^9$ /mL [57] (both NTA). Isolation by SEC yielded  $\langle n \rangle$  between  $10 \times 10^9$ /mL [64] and  $4975.6 \times 10^9$ /mL [58] (both NTA), and precipitation/membrane-based affinity yielded results between  $7.6 \times 10^9$ /mL [69] and  $7383 \times 10^9$ /mL [57] (both NTA). Overall, the results presented in Table 5 span seven orders of magnitude, from  $0.0002 \times 10^9$ /mL (diluted plasma, FCM) to  $7383 \times 10^9$ /mL (precipitation, NTA). This observation exceeds the notion of Johnsen et al. (2019), who reported that the EV number density in plasma spans six orders of magnitude, depending on the harvesting and measurement methods [70]. The results presented in Table 5 confirm that  $\langle n \rangle$  of EPs strongly depends on the sample preparation and assessment methods.

The method of harvesting the EPs is also important in the determination of the size, as different methods harvest different populations of particles. We estimated the size of the EPs directly in diluted blood by  $\langle D_h \rangle$  (146 nm), whereas Marchisio et al. (2021) estimated the size to be larger than 160 nm using FCM [38]. Directly in diluted plasma, the estimated  $\langle D_h \rangle$  were between 20 nm (DLS [23]) and 266 nm (DLS [20]). In isolates obtained using UC, the estimated  $\langle D_h \rangle$  were between 70 nm (NTA [35,56]) and 208 nm (NTA [57]). For SEC, the estimated  $\langle D_h \rangle$  were between 70 nm (TRPS [65]) and 202 nm (NTA [66]). Precipitation/membrane-based affinity yielded  $\langle D_h \rangle$  between 77 nm (DLS [57]) and 238 nm (NTA [55]). For TEM, the assessed sizes were between 87 and 112 nm [60]. Overall, the average estimated sizes were between 20 nm and 234 nm, which is a much smaller interval than the range of  $\langle n \rangle$ ,  $(0.00004\text{--}7383) \times 10^9$ /mL. In determining the size, the instruments limit the interval of the possible size results; however, in principle, sizes larger than 250 nm can be assessed by ILM, DLS, NTA, and TEM. Although the distributions of the individual measurements were subject to finite widths that were much larger than the standard deviations of the repeated measurements (e.g., Figure 2, panels (d)–(g)), in Table 5, all of the reported  $\langle D_h \rangle$  are smaller than 250 nm.

The batch techniques ILM, NTA, DLS, and TRPS generally do not distinguish different types of EPs in samples. It was suggested that lipoproteins are the main type of lipid particles in blood-derived samples [71–74]. The sizes of the lipoproteins assessed by nuclear magnetic resonance imaging of 27673 blood samples [75] were 21 nm for low-density lipoproteins, 9 nm for high-density lipoproteins, and 47–49 nm for very low-density lipoproteins. ILM does not detect particles smaller than about 80 nm (e.g., lipoproteins) and larger than about 500 nm (e.g., cells), which is well-suited for the detection of EPs. Because of their size range, lipoproteins do not interfere with the measurement of EPs using instruments with a threshold of approximately 80 nm [76]. However, lipoproteins may interact with EPs [72,73]. In addition, a protein corona can form on EPs [77,78], and complexes cannot be distinguished from undecorated EPs with existing batch methods [72–74]. Moreover, the proportion of lipoproteins in a sample may depend on the harvesting method [76,79,80]. György et al. (2010) pointed to the presence of immune complexes in samples and suggested using lysis of membrane-enclosed vesicles with detergent to quantify the respective populations [76].

#### 4.5. Outlines and Perspectives

In spite of the expected high noise with harvesting and assessment procedures (as reflected in the large standard deviations), the measured and corrected values of  $\langle n \rangle$  in the human plasma and blood were remarkably similar (Tables 3 and 4). The samples in plasma and blood showed statistically significant correlations (Figure 1, Table 1), which indicates that a considerable portion of the EPs in the plasma also constituted the population of EPs in the blood—or were derived from EPs in the blood. This shows that the properties of the samples, not just the limitations of the instruments, contributed to the results. In the canine samples, we found no statistically significant correlation between  $n$  in the plasma and  $n$  in the blood; in our opinion, this was due to the too high blood dilution imposed for all canine blood samples, resulting in high levels of noise in the measurements of blood EPs. Accordingly, greater scattering in the  $D_h(n)$  dependence in the canine blood (Figure 1c, empty circles) can be noted compared to the human blood (Figure 1b).

We found no statistically significant differences between respective  $\langle n \rangle$  or  $\langle D_h \rangle$  in the populations of samples with the two anticoagulants (trisodium citrate and EDTA) (Tables 2 and 3), neither in human plasma nor in human blood (Table 2), and the correlations between the respective parameters in the samples with trisodium citrate and EDTA were statistically significant (Table 1). This indicates that, at a population level, the choice between trisodium citrate and EDTA did not have an impact—as previously observed by Bettio et al. (2023) [55].

We found statistically significant differences with sufficient statistical power between  $\langle D_h \rangle$  in the plasma and blood in human and in the dog (Table 2). The EPs were, on average, larger in the blood than in the plasma (Table 2). All reported correlations of  $D_h$  were statistically significant.

Although our results obtained from diluted blood exhibit greater scattering than those in diluted plasma (Figure 1), we think that improvement in the preparation of samples (in particular, measurement directly in diluted blood) could enable a critical number of population studies to achieve sufficient statistical power and also clinical relevance—thereby paving the way for clinically relevant assessments of the number density and size of EPs. The dilution of blood seems to be the least detrimental of all procedures aimed at assessing the number density and size of EPs in blood. We outline the analysis of EPs in a multicenter prospective study by Brocco et al. (2022), who demonstrated higher  $\langle n \rangle$  and  $\langle D_h \rangle$  of EPs in diluted blood from 56 patients with pancreatic cancer compared with 48 healthy individuals [39]. The use of FCM in this study employed fluorescence marking of EPs to quantify the subpopulations of EPs and relate the results to clinical outcomes [39]. However, the preparation of plasma and assessment of EPs in plasma remain of interest, as plasma is widely used in different fields of medicine for regeneration [81,82].

Although EPs in human IBD have previously been considered [83–88], to the best of our knowledge, we are the first to report on EPs in canine BOAS. As the interest in the application of EPs in veterinary medicine is expanding [89], it is expected that the study of animal samples will reveal important information about the general properties of EPs.

#### 4.6. Challenges and Approaches

The International Society for Extracellular Vesicles (ISEV) is currently addressing the nomenclature, methods of harvesting, and the characterization of EPs, as well as conducting functional studies with various biological samples, to strengthen the approach to challenges related to EPs and to facilitate communication among scientists working in this multidisciplinary field. The ISEV recently published an update on the minimal information required for studies on extracellular vesicles [4], and the ISEV Blood EV Task Force created the Minimal Information for Blood EV Research (MIBlood-EV) [4], a tool to record and report information about pre-analytical protocols used for plasma and serum preparation, as well as the assays used to assess the quality of these preparations [90]. As all currently applied methods are subject to significant limitations, a combination of methods that exploit different physical and biochemical properties is recommended. However, the search for improved methods continues. ILM is a recently introduced method, which was hitherto used to detect viruses [26,27,91,92], phages [26,29], liposomes [28,93], and EPs [28,44,94,95]. Furthermore, interferometric NTA based on a laser light source offers the possibility of a better resolution down to smaller EP sizes [96]. Sausset et al. (2023) compared the performances of different techniques (ILM, TEM, and NTA) in the determination of the size of EPs isolated from bacteria, feces, bovine milk, and human cells, as well as phages of various sizes and shapes [29]. ILM performed well above its threshold 80 nm and it was suggested that ILM could be advantageous for large cohort studies, as the measurement is faster, simpler, and cheaper than NTA [29]. Our results are in favor of these suggestions; with our choice of protocols and equipment, we have assessed more than 700 samples in one year from patients included in the ongoing clinical studies, which is to our knowledge the largest number of EPs yet processed within a single design and setting.

In plasma and, particularly, in blood, there are also other particles besides EPs (e.g., lipoproteins, protein complexes, and cells). Although singular smaller particles are out of detection range of ILM, their group configuration could induce a fake signal, as previously observed for FCM [72,97]. In seeking the appropriate dilution of the samples, we observed that sometimes the signal was under the detection limit, but with increased dilution, the instrument was able to detect the particles, which aligns with FCM results detecting more particles with the dilution of samples [97]. The so-called swarm effect could explain the steep increase in the  $D_h(n)$  curve with the decrease in  $n$  (Figure 1a–c). However, we observed on the camera display that ILM also detects signals moving synchronously with the cells. EPs could either be adhered to the cells or the cells exhibit protrusions of a size similar to the EPs. As cells are larger and less mobile than EPs, Brownian motion of the particle is hindered and  $D_h$  determined by the Stokes–Einstein relation overestimates the size of such particles. These artefacts were stronger in the blood than in the plasma, both in human and in the dog (Figures 1b and 1c, respectively), and this could have contributed to larger  $\langle D_h \rangle$  in the blood than in the respective plasma (Table 2).

Although  $D_h$  and  $n$  are important measures to determine whether a sample preparation procedure affects EVs, they are insufficient to characterize whether that changes the EV internal content or membrane. Complementary techniques are needed to obtain information on such mechanisms regarding EPs and surrounding media (e.g., proteomic analysis [98–101]), as well as potential biological impacts. However, the complementary techniques should be subject to the same preparation of the sample.

## 5. Conclusions

To overcome the bottleneck to clinical relevance (formed by lengthy, sophisticated, deleterious, and poorly repeatable procedures that are invasive to samples), we analyzed

populations of samples derived from clinical studies on two species (human and dog) for  $n$  and  $D_h$  by means of ILM. We experienced that the assessment of larger number of samples within populations by means of ILM is feasible. We found strong  $n$  and  $D_h$  correlations within and between human plasma and blood and between  $D_h$  in canine plasma and blood. We observed no statistically significant differences in the average number densities between the human samples. The value of  $\langle D_h \rangle$  was statistically significantly larger in blood than in plasma in human and in the dog. With ILM, improvements in the preparation of samples are needed, particularly for blood (e.g., personalized preparation of plasma and optimized dilution of plasma and of blood). To better understand the mechanisms taking place during processing of samples and to improve the methods, biophysical considerations of EPs will be highly warranted in the future.

**Supplementary Materials:** The following supporting information can be downloaded at: <https://www.mdpi.com/article/10.3390/cells13242054/s1>, The raw data are available in Korenjak, B., Tratenšek, A., Arko, M., Romolo, A., Berry, M., Drobne, D., Vovk, T., Igljč, A., Nemec Svete, A., Erjavec, V., & Kralj-Igljč, V. (2024). Raw Data on Extracellular Particles in 613 Human and 163 Canine Diluted Plasma and Blood Samples Assessed by Interferometric Light Microscopy (1.0.0) [Data set]. Zenodo. <https://doi.org/10.5281/zenodo.14015248>.

**Author Contributions:** Conceptualization, V.K.-I., V.E., T.V. and D.D.; methodology, V.K.-I., A.N.S., M.K., M.H., A.B.Z. and B.K.; software, B.K., M.A. and A.R.; validation, V.K.-I.; formal analysis, B.K., A.T., M.A., M.B., A.R., M.K., M.H. and V.K.-I.; investigation, all coauthors; resources, V.K.-I., D.D., T.V., A.I., A.N.S. and V.E.; data curation, B.K., M.A., M.B., A.R. and V.K.-I.; writing—original draft preparation, B.K., A.R. and V.K.-I.; writing—review and editing, all authors; visualization, M.H., M.K., B.K., M.B. and V.K.-I.; supervision, V.K.-I., A.I. and V.E.; project administration, V.K.-I. and A.I.; funding acquisition, D.D., T.V., A.I., A.N.S., V.E. and V.K.-I. All authors have read and agreed to the published version of the manuscript.

**Funding:** This research was funded by Slovenian Research Agency (ARIS) (grant numbers: J3-3066, J2-4447, J3-4499, P1-0189, P1-0391, P2-0132, P2-0232, P3-0388, P4-0053, and project Nanostrukturome according to a contract between ARIS and University of Ljubljana); the Ministry of Innovation and Technology of Hungary, from the National Research, Development, and Innovation Fund (grant number: SNN 138407); and the European Union's Horizon 2020 Research and Innovation Programme under the Marie Skłodowska-Curie Staff Exchange project "FarmEVs" (grant agreement no: 101131175). The views and opinions expressed in this publication are solely those of the authors and do not necessarily reflect those of the European Union. Neither the European Union nor the granting authority can be held responsible. Some of this work was performed at the National Institute of Chemistry Cryo-EM Facility, supported by the Slovenian Research Agency Infrastructure Programme IO-0003.

**Institutional Review Board Statement:** The human study was conducted in accordance with the Declaration of Helsinki and approved by the National Medical Ethics Committee of the Republic of Slovenia (0120-271/2022/4; KME 27 July 2022). All procedures in the animal study complied with Slovenian government regulations (Animal Protection Act, Official Gazette of the Republic of Slovenia, No. 43/2007). The animal study was approved by the Animals in Experiments Welfare Commission of the Veterinary Faculty, University of Ljubljana, approval number: 18-3/2022-1.

**Informed Consent Statement:** Written informed consent was provided by the human blood donors and by the owners of the animals.

**Data Availability Statement:** The raw data are provided in the Supplementary Materials.

**Conflicts of Interest:** The authors declare no conflicts of interest.

## References

1. Wolf, P. The nature and significance of platelet products in human plasma. *Br. J. Haematol.* **1967**, *13*, 269–288. [[CrossRef](#)] [[PubMed](#)]
2. Romolo, A.; Kralj-Igljč, V. Milestones in Research of Small Cellular Particles. Membrane Modeling and Theoretical Description in Connection with in vitro and ex vivo processes. *Proc. Socrat. Lect.* **2024**, *10*, 59–68. [[CrossRef](#)]



3. Yáñez-Mó, M.; Siljander, P.R.; Andreu, Z.; Zavec, A.B.; Borràs, F.E.; Buzas, E.I.; Buzas, K.; Casal, E.; Cappello, F.; Carvalho, J.; et al. Biological properties of extracellular vesicles and their physiological functions. *J. Extracell. Ves.* **2015**, *4*, 27066. [[CrossRef](#)] [[PubMed](#)]
4. Welsh, J.A.; Goberdhan, D.C.I.; O'Driscoll, L.; Buzas, E.I.; Blenkiron, C.; Bussolati, B.; Cai, H.; Di Vizio, D.; Driedonks, T.A.P.; Erdbrügger, U.; et al. Minimal information for studies of extracellular vesicles (MISEV2023): From basic to advanced approaches. *J. Extracell. Ves.* **2024**, *13*, e12404. [[CrossRef](#)] [[PubMed](#)]
5. Rai, A.; Claridge, B.; Lozano, J.; Greening, D.W. The Discovery of Extracellular Vesicles and Their Emergence as a Next-Generation Therapy. *Circ. Res.* **2024**, *135*, 198–221. [[CrossRef](#)]
6. Cui, L.; Perini, G.; Palmieri, V.; De Spirito, M.; Papi, M. Plant-Derived Extracellular Vesicles as a Novel Frontier in Cancer Therapeutics. *Nanomater* **2024**, *14*, 1331. [[CrossRef](#)]
7. Hägerstrand, H.; Isomaa, B. Vesiculation induced by amphiphiles in erythrocytes. *Biochim. Biophys. Acta* **1989**, *982*, 179–186. [[CrossRef](#)]
8. Junkar, I.; Šuštar, V.; Frank, M.; Janša, V.; Bedina Zavec, A.; Rozman, B.; Mozetic, M.; Hägerstrand, H.; Kralj-Iglič, V. Blood and sinovial microparticles as revealed by atomic force and scanning electron microscope. *Open Autoimm. J.* **2009**, *1*, 50–58. [[CrossRef](#)]
9. Mrvar-Brečko, A.; Šuštar, V.; Janša, V.; Štukelj, R.; Janša, R.; Mujagić, E.; Kruljč, P.; Hägerstrand, H.; Iglič, A.; Kralj-Iglič, V. Isolated microvesicles from peripheral blood and body fluids as observed by scanning electron microscope. *Blood Cells Mol. Dis.* **2010**, *44*, 307–312. [[CrossRef](#)]
10. Kralj-Iglič, V.; Pocsfalvi, G.; Mesarec, L.; Šuštar, V.; Hägerstrand, H.; Iglič, A. Minimizing isotropic and deviatoric membrane energy—An unifying formation mechanism of different cellular membrane nanovesicle types. *PLoS ONE* **2020**, *15*, e0244796. [[CrossRef](#)]
11. Hägerstrand, H.; Bobrowska-Hägerstrand, M.; Lillsunde, I.; Isomma, B. Vesiculation induced by amphiphiles and ionophore A23187 in porcine platelets: A transmission electron microscopic study. *Chem. Biol. Interact.* **1996**, *101*, 115–126. [[CrossRef](#)] [[PubMed](#)]
12. Pisitkun, T.; Shen, R.F.; Knepper, M.A. Identification and proteomic profiling of exosomes in human urine. *Proc. Natl. Acad. Sci. USA* **2004**, *101*, 13368–13373. [[CrossRef](#)]
13. Szatanek, R.; Baj-Krzyworzeka, M.; Zimoch, J.; Lekka, M.; Siedlar, M.; Baran, J. The Methods of Choice for Extracellular Vesicles (EVs) Characterization. *Int. J. Mol. Sci.* **2017**, *18*, 1153. [[CrossRef](#)] [[PubMed](#)]
14. Jung, M.K.; Mun, J.Y. Sample Preparation and Imaging of Exosomes by Transmission Electron Microscopy. *J. Vis. Exp.* **2018**, *131*, 56482. [[CrossRef](#)]
15. Brisson, A.R.; Tan, S.; Linares, R.; Gounou, C.; Arraud, N. Extracellular vesicles from activated platelets: A semiquantitative cryo-electron microscopy and immuno-gold labeling study. *Platelets* **2017**, *3*, 263–271. [[CrossRef](#)] [[PubMed](#)]
16. Božič, D.; Hočevár, M.; Kisovec, M.; Pajnič, M.; Paden, L.; Jeran, M.; Bedina Zavec, A.; Podobnik, M.; Kogej, K.; Iglič, A.; et al. Stability of Erythrocyte-Derived Nanovesicles Assessed by Light Scattering and Electron Microscopy. *Int. J. Mol. Sci.* **2021**, *22*, 12772. [[CrossRef](#)]
17. Dittrich, W.; Gohde, W. Impulse Fluorometry of Single Cells in Suspension. Teil B, Chemie, Biochemie, Biophysik, Biologie und Verwandte Gebiete. *Z. Naturforsch. B* **1969**, *24*, 360–361.
18. Lacroix, R.; Robert, S.; Poncelet, P.; Kasthuri, R.S.; Key, N.S.; Dignat-George, F.; ISTH SSC Workshop. Standardization of platelet-derived microparticle enumeration by flow cytometry with calibrated beads: Results of the International Society on Thrombosis and Haemostasis SSC Collaborative workshop. *J. Thromb. Haemost.* **2010**, *8*, 2571–2574. [[CrossRef](#)]
19. Welsh, J.A.; Arkesteijn, G.J.A.; Bremer, M.; Cimorelli, M.; Dignat-George, F.; Giebel, B.; Görgens, A.; Hendrix, A.; Kuiper, M.; Lacroix, R.; et al. A compendium of single extracellular vesicle flow cytometry. *J. Extracell. Vesicles* **2023**, *12*, e12299. [[CrossRef](#)] [[PubMed](#)]
20. Lawrie, A.S.; Albanyan, A.; Cardigan, R.A.; Mackie, I.J.; Harrison, P. Microparticle sizing by dynamic light scattering in fresh-frozen plasma. *Vox Sang.* **2009**, *4*, 206–212. [[CrossRef](#)] [[PubMed](#)]
21. Wu, S.; Zhao, Y.; Zhang, Z.; Zuo, C.; Wu, H.; Liu, Y. The Advances and Applications of Characterization Technique for Exosomes: From Dynamic Light Scattering to Super-Resolution Imaging Technology. *Photonics* **2024**, *11*, 101. [[CrossRef](#)]
22. Božič, D.; Sitar, S.; Junkar, I.; Štukelj, R.; Pajnič, M.; Žagar, E.; Kralj-Iglič, V.; Kogej, K. Viscosity of plasma as a key factor in assessment of extracellular vesicles by light scattering. *Cells* **2019**, *8*, 1046. [[CrossRef](#)] [[PubMed](#)]
23. Kogej, K.; Božič, D.; Kobal, B.; Herzog, M.; Černe, K. Application of Dynamic and Static Light Scattering for Size and Shape Characterization of Small Extracellular Nanoparticles in Plasma and Ascites of Ovarian Cancer Patients. *Int. J. Mol. Sci.* **2021**, *22*, 12946. [[CrossRef](#)] [[PubMed](#)]
24. Carr, R.; Hole, P.; Malloy, A.; Nelson, P.; Wright, M.; Smith, J. Applications of nanoparticle tracking analysis in nanoparticle research—A mini-review. *Eur. J. Parenter. Pharm. Sci.* **2009**, *14*, 45–50.
25. Dragovic, R.A.; Gardiner, C.; Brooks, A.S.; Tannetta, D.S.; Ferguson, D.J.; Hole, P.; Carr, B.; Redman, C.W.; Harris, A.L.; Dobson, P.J.; et al. Sizing and phenotyping of cellular vesicles using nanoparticle tracking analysis. *Nanomedicine* **2011**, *7*, 780–788. [[CrossRef](#)]
26. Boccara, M.; Fedala, Y.; Vénien-Bryan, C.; Bailly-Bechet, M.; Bowler, C.; Boccara, A.C. Full-field interferometry for counting and differentiating aquatic biotic nanoparticles: From laboratory to Tara Oceans. *Biomed. Opt. Express* **2016**, *7*, 3736–3746. [[CrossRef](#)]

27. Roose-Amsaleg, C.; Fedala, Y.; Vénien-Bryan, C.; Garnier, J.; Boccara, A.C.; Boccara, M. Utilization of interferometric light microscopy for the rapid analysis of virus abundance in a river. *Res. Microbiol.* **2017**, *168*, 413–418. [[CrossRef](#)]
28. Romolo, A.; Jan, Z.; Bedina Zavec, A.; Kisovec, M.; Arrigler, V.; Spasovski, V.; Podobnik, M.; Igljč, A.; Pocsfalvi, G.; Kogej, K.; et al. Assessment of Small Cellular Particles from Four Different Natural Sources and Liposomes by Interferometric Light Microscopy. *Int. J. Mol. Sci.* **2022**, *23*, 15801. [[CrossRef](#)]
29. Sausset, R.; Krupova, Z.; Guédon, E.; Peron, S.; Grangier, A.; Petit, M.A.; De Sordi, L.; De Paepe, M. Comparison of interferometric light microscopy with nanoparticle tracking analysis for the study of extracellular vesicles and Bacteriophages. *J. Extracell. Biol.* **2023**, *2*, 75. [[CrossRef](#)]
30. Coulter, W.H. Means for Counting Particles Suspended in a Fluid. U.S. Patent 2656508A, 20 October 1953.
31. De Blois, R.W.; Wesley, R.K. Sizes and concentrations of several type C oncornaviruses and bacteriophage T2 by the resistive-pulse technique. *J. Virol.* **1977**, *23*, 227–233. [[CrossRef](#)]
32. Maas, S.L.; De Vrij, J.; Broekman, M.L. Quantification and size-profiling of extracellular vesicles using tunable resistive pulse sensing. *J. Vis. Exp.* **2014**, *92*, 51623. [[CrossRef](#)]
33. Maas, S.L.; Broekman, M.; de Vrij, J. Tunable Resistive Pulse Sensing for the Characterization of Extracellular Vesicles. *Methods Mol. Biol.* **2017**, *1545*, 21–33. [[CrossRef](#)] [[PubMed](#)]
34. Varga, Z.; Yuana, Y.; Grootemaat, A.E.; van der Pol, E.; Gollwitzer, C.; Krumrey, M.; Nieuwland, R. Towards traceable size determination of extracellular vesicles. *J. Extracell. Vesicles* **2014**, *4*, 3. [[CrossRef](#)] [[PubMed](#)]
35. Gardiner, C.; Ferreira, Y.J.; Dragovic, R.A.; Redman, C.W.; Sargent, I.L. Extracellular vesicle sizing and enumeration by nanoparticle tracking analysis. *J. Extracell. Vesicles* **2013**, *2*, 10. [[CrossRef](#)] [[PubMed](#)]
36. Božič, D.; Hočevar, M.; Kononenko, V.; Jeran, M.; Štibler, U.; Fiume, I.; Pajnič, M.; Pađen, L.; Kogej, K.; Drobne, D.; et al. Pursuing mechanisms of extracellular vesicle formation. Effects of sample processing. In *Advances in Biomembranes and Lipid Self-Assembly*; Bongiovanni, A., Pocsfalvi, G., Manno, M., Kralj-Igljč, V., Eds.; Elsevier: Amsterdam, The Netherlands, 2020; Volume 32, pp. 113–155. [[CrossRef](#)]
37. Šuštar, V.; Bedina Zavec, A.; Štukelj, R.; Frank, M.; Bobojevič, G.; Janša, R.; Ogorevc, E.; Kruljc, P.; Mam, K.; Šimunič, B.; et al. Nanoparticles isolated from blood—a reflection of vesiculability of blood cells during the isolation process. *Int. J. Nanomed.* **2011**, *6*, 2737–2748. [[CrossRef](#)]
38. Marchisio, M.; Simeone, P.; Bologna, G.; Ercolino, E.; Pierdomenico, L.; Pieragostino, D.; Ventrella, A.; Antonini, F.; Del Zotto, G.; Vergara, D.; et al. Flow Cytometry Analysis of Circulating Extracellular Vesicle Subtypes from Fresh Peripheral Blood Samples. *Int. J. Mol. Sci.* **2021**, *22*, 48. [[CrossRef](#)]
39. Brocco, D.; De Bellis, D.; Di Marino, P.; Simeone, P.; Grassadonia, A.; De Tursi, M.; Grottola, T.; Di Mola, F.F.; Di Gregorio, P.; Zappacosta, B.; et al. High Blood Concentration of Leukocyte-Derived Extracellular Vesicles Is Predictive of Favorable Clinical Outcomes in Patients with Pancreatic Cancer: Results from a Multicenter Prospective Study. *Cancers* **2022**, *14*, 4748. [[CrossRef](#)]
40. Robinson, S.D.; Samuels, M.; Jones, W.; Stewart, N.; Eravci, M.; Mazarakis, N.K.; Gilbert, D.; Critchley, G.; Glamis, G. Confirming size-exclusion chromatography as a clinically relevant extracellular vesicles separation method from 1mL plasma through a comprehensive comparison of methods. *BMC Methods* **2024**, *1*, 7. [[CrossRef](#)]
41. Mork, M.; Pedersen, S.; Botha, J.; Lund, S.M.; Kristensen, S.R. Preanalytical, analytical, and biological variation of blood plasma submicron particle levels measured with nanoparticle tracking analysis and tunable resistive pulse sensing. *Scand. J. Clin. Lab. Investig.* **2016**, *76*, 349–360. [[CrossRef](#)]
42. de Vrij, J.; Maas, S.L.; van Nispen, M.; Sena-Esteves, M.; Limpens, R.W.; Koster, A.J.; Leenstra, S.; Lamfers, M.L.; Broekman, M.L. Quantification of nanosized extracellular membrane vesicles with scanning ion occlusion sensing. *Nanomedicine* **2013**, *8*, 1443–1458. [[CrossRef](#)]
43. Botha, J.; Pugsley, H.R.; Handberg, A. Conventional, High-Resolution and Imaging Flow Cytometry: Benchmarking Performance in Characterisation of Extracellular Vesicles. *Biomedicines* **2021**, *9*, 124. [[CrossRef](#)]
44. Berry, M.; Arko, M.; Romolo, A.; Brložnik, M.; Mrvar Brečko, A.; Korenjak, B.; Igljč, A.; Kadunc Kos, V.; Kruljc, P.; Nemeč Svete, A.; et al. Validation of Interferometric Light Microscopy for Assessment of Extracellular Particles in Diluted Plasma: Preparing the Path for Future Clinical Practices. *Proc. Socrat. Lect. 10th* **2024**, *10*, 54–58. [[CrossRef](#)]
45. Lilja-Maula, L.; Lappalainen, A.K.; Hyytiäinen, H.K.; Kuusela, E.; Kaimio, M.; Schildt, K.; Mölsä, S.; Morelius, M.; Rajamäki, M.M. Comparison of submaximal exercise test results and severity of brachycephalic obstructive airway syndrome in English bulldogs. *Vet. J.* **2017**, *219*, 22–26. [[CrossRef](#)]
46. Vozel, D.; Uršič, B.; Krek, J.L.; Štukelj, R.; Kralj-Igljč, V. Applicability of extracellular vesicles in clinical studies. *Eur. J. Clin. Investig.* **2017**, *47*, 305–313. [[CrossRef](#)]
47. Božič, D.; Vozel, D.; Hočevar, M.; Jeran, M.; Jan, Z.; Pajnič, M.; Pađen, L.; Igljč, A.; Battelino, S.; Kralj-Igljč, V. Enrichment of plasma in platelets and extracellular vesicles by the counterflow to erythrocyte settling. *Platelets* **2022**, *33*, 592–602. [[CrossRef](#)]
48. Štukelj, R.; Hribar Ignasčenko, I.; Peternelj, S.; Peruško, M.; Blažič, T.; Pajnič, M.; Bračun Vnuk, Š.; Šuštar, V.; Bedina Zavec, A.; Schara, K.; et al. Role of blood sampling in assessment of concentration of extracellular nanovesicles in isolates from peripheral blood. In *Advances in Planar Lipid Bilayers and Liposomes*; Elsevier: Amsterdam, The Netherlands, 2014; Volume 19, pp. 175–189. [[CrossRef](#)]

49. Štukelj, R.; Schara, K.; Bedina-Zavec, A.; Šuštar, V.; Pajnič, M.; Pađen, L.; Krek, J.L.; Kralj-Iglič, V.; Mrvar-Brečko, A.; Janša, R. Effect of the shear stress in the flow through the sampling needle on concentration of nanovesicles isolated from blood. *Eur. J. Pharm. Sci.* **2017**, *98*, 17–29. [[CrossRef](#)]
50. Filipe, V.; Hawe, A.; Jiskoot, W. Critical evaluation of Nanoparticle Tracking Analysis (NTA) by NanoSight for the measurement of nanoparticles and protein aggregates. *Pharm. Res.* **2010**, *27*, 796–810. [[CrossRef](#)]
51. Kim, A.; Ng, W.B.; Bernt, W.; Cho, N.J. Validation of Size Estimation of Nanoparticle Tracking Analysis on Polydisperse Macromolecule Assembly. *Sci. Rep.* **2019**, *9*, 2639. [[CrossRef](#)]
52. Holcar, M.; Marić, I.; Tertel, T.; Goričar, K.; Černe, D.; Giebel, B.; Lenassi, M. Comprehensive Phenotyping of Extracellular Vesicles in Blood of Healthy Humans—Insights into Cellular Origin and Biological Variability. *bioRxiv* **2024**, 1–39. Available online: <https://www.biorxiv.org/content/10.1101/2024.07.04.602156v1.full.pdf> (accessed on 28 October 2024).
53. Elgamal, S.; Cocucci, E.; Sass, E.J.; Mo, X.M.; Blissett, A.R.; Calomeni, E.P.; Rogers, K.A.; Woyach, J.A.; Bhat, S.A.; Muthusamy, N.; et al. Optimizing extracellular vesicles' isolation from chronic lymphocytic leukemia patient plasma and cell line supernatant. *J. Clin. Investig.* **2021**, *6*, e137937. [[CrossRef](#)]
54. Osti, D.; Del Bene, M.; Rappa, G.; Santos, M.; Matafora, V.; Richichi, C.; Faletti, S.; Beznoussenko, G.V.; Mironov, A.; Bachi, A.; et al. Clinical Significance of Extracellular Vesicles in Plasma from Glioblastoma Patients. *Clin. Cancer Res.* **2019**, *25*, 266–276. [[CrossRef](#)]
55. Bettio, V.; Mazzucco, E.; Antona, A.; Cracas, S.; Valarda, M.; Venetucci, J.; Bruno, S.; Chiabotto, G.; Venegoni, C.; Vasile, A.; et al. Extracellular vesicles from human plasma for biomarkers discovery: Impact of anticoagulants and isolation techniques. *PLoS ONE* **2023**, *18*, e0285440. [[CrossRef](#)]
56. Jamaly, S.; Ramberg, C.; Olsen, R.; Latysheva, N.; Webster, P.; Sovershaev, T.; Brækkan, S.K.; Hansen, J.B. Impact of preanalytical conditions on plasma concentration and size distribution of extracellular vesicles using Nanoparticle Tracking Analysis. *Sci. Rep.* **2018**, *8*, 17216. [[CrossRef](#)]
57. Serrano-Pertierra, E.; Oliveira-Rodríguez, M.; Rivas, M.; Oliva, P.; Villafani, J.; Navarro, A.; Blanco-López, M.C.; Cernuda-Morollón, E. Characterization of Plasma-Derived Extracellular Vesicles Isolated by Different Methods: A Comparison Study. *Bioengineering* **2019**, *6*, 8. [[CrossRef](#)]
58. Malys, M.S.; Aigner, C.; Schulz, S.M.; Schachner, H.; Rees, A.J.; Kain, R. Isolation of Small Extracellular Vesicles from Human Sera. *Int. J. Mol. Sci.* **2021**, *22*, 4653. [[CrossRef](#)]
59. George, S.K.; Lauková, L.; Weiss, R.; Semak, V.; Fendl, B.; Weiss, V.U.; Steinberger, S.; Allmaier, G.; Tripisciano, C.; Weber, V. Comparative Analysis of Platelet-Derived Extracellular Vesicles Using Flow Cytometry and Nanoparticle Tracking Analysis. *Int. J. Mol. Sci.* **2021**, *22*, 3839. [[CrossRef](#)]
60. Scavo, M.P.; Cigliano, A.; Depalo, N.; Fanizza, E.; Bianco, M.G.; Denora, N.; Laquintana, V.; Curri, M.L.; Lorusso, D.; Lotesoriere, C.; et al. Frizzled-10 Extracellular Vesicles Plasma Concentration Is Associated with Tumoral Progression in Patients with Colorectal and Gastric Cancer. *J. Oncol.* **2019**, *2019*, 2715968. [[CrossRef](#)]
61. Długolecka, M.; Szymanski, J.; Zareba, L.; Homoncik, Z.; Domagala-Kulawik, J.; Polubiec-Kownacka, M.; Czystowska-Kuzmicz, M. Characterization of Extracellular Vesicles from Bronchoalveolar Lavage Fluid and Plasma of Patients with Lung Lesions Using Fluorescence Nanoparticle Tracking Analysis. *Cells* **2021**, *10*, 3473. [[CrossRef](#)]
62. Picciolini, S.; Alice Gualerzi, A.; Carlomagno, C.; Cabinio, M.; Sorrentino, S.; Baglio, F.; Bedoni, M. An SPRI-based biosensor pilot study: Analysis of multiple circulating extracellular vesicles and hippocampal volume in Alzheimer's disease. *J. Pharm. Anal.* **2021**, *192*, 113649. [[CrossRef](#)]
63. Contreras, H.; Alarcón-Zapata, P.; Nova-Lamperti, E.; Ormazabal, V.; Varas-Godoy, M.; Salomon, C.; Zuniga, F.A. Comparative study of size exclusion chromatography for isolation of small extracellular vesicle from cell-conditioned media, plasma, urine, and saliva. *Front. Nanotechnol.* **2023**, *5*, 1146772. [[CrossRef](#)]
64. Stranska, R.; Gysbrechts, L.; Wouters, J.; Vermeersch, P.; Bloch, K.; Dierickx, D.; Andrei, G.; Snoeck, R. Comparison of membrane affinity-based method with size-exclusion chromatography for isolation of exosome-like vesicles from human plasma. *J. Transl. Med.* **2018**, *16*, 1–9. [[CrossRef](#)]
65. Diehl, J.N.; Ray, A.; Collins, L.B.; Peterson, A.; Alexander, K.C.; Boutros, J.G.; Ikonomidis, J.S.; Akerman, A.W. A standardized method for plasma extracellular vesicle isolation and size distribution analysis. *PLoS ONE* **2023**, *4*, 18. [[CrossRef](#)]
66. Franco, C.; Ghirardello, A.; Bertazza, L.; Gasparotto, M.; Zanatta, E.; Iaccarino, L.; Valadi, H.; Doria, A.; Gatto, M. Size-Exclusion Chromatography Combined with Ultrafiltration Efficiently Isolates Extracellular Vesicles from Human Blood Samples in Health and Disease. *Int. J. Mol. Sci.* **2023**, *24*, 3663. [[CrossRef](#)]
67. Longobardi, A.; Benussi, L.; Nicsanu, R.; Bellini, S.; Ferrari, C.; Saraceno, C.; Zanardini, R.; Catania, M.; Di Fede, G.; Squitti, R.; et al. Plasma Extracellular Vesicle Size and Concentration Are Altered in Alzheimer's Disease, Dementia With Lewy Bodies, and Frontotemporal Dementia. *Front. Cell Dev. Biol.* **2021**, *9*, 667369. [[CrossRef](#)]
68. König, L.; Kasimir-Bauer, S.; Bittner, A.K.; Hoffmann, O.; Wagner, B.; Santos Manvailer, L.F.; Kimmig, R.; Horn, P.A.; Rebmann, V. Elevated levels of extracellular vesicles are associated with therapy failure and disease progression in breast cancer patients undergoing neoadjuvant chemotherapy. *Oncimmunology* **2017**, *7*, e1376153. [[CrossRef](#)]
69. Giloteaux, L.; O'Neal, A.; Castro-Marrero, J.; Levine, S.M.; Hanson, M.R. Cytokine profiling of extracellular vesicles isolated from plasma in myalgic encephalomyelitis/chronic fatigue syndrome: A pilot study. *J. Transl. Med.* **2020**, *18*, 387. [[CrossRef](#)]

70. Johnsen, K.B.; Gudbergsson, J.M.; Andresen, T.L.; Simonsen, J.B. What is the blood concentration of extracellular vesicles? Implications for the use of extracellular vesicles as blood-borne biomarkers of cancer. *Biochim. Biophys. Acta* **2019**, *1871*, 109–116. [[CrossRef](#)]
71. German, J.B.; Smilowitz, J.T.; Zivkovic, A.M. Lipoproteins: When size really matters. *Curr. Opin. Colloid Interface Sci.* **2006**, *11*, 171–183. [[CrossRef](#)]
72. Sódar, B.W.; Kittel, Á.; Pálóczi, K.; Vukman, K.V.; Osteikoetxea, X.; Szabó-Taylor, K.; Németh, A.; Sperlágh, B.; Baranyai, T.; Giricz, Z.; et al. Low-density lipoprotein mimics blood plasma-derived exosomes and microvesicles during isolation and detection. *Sci. Rep.* **2016**, *6*, 24316. [[CrossRef](#)]
73. Kuchinskiene, Z.; Carlson, L.A. Composition, concentration, and size of low density lipoproteins and of subfractions of very low density lipoproteins from serum of normal men and women. *J. Lipid Res.* **1982**, *23*, 762–769. [[CrossRef](#)] [[PubMed](#)]
74. Nieuwland, R.; Siljander, P.R. A beginner's guide to study extracellular vesicles in human blood plasma and serum. *J. Extracell. Vesicles* **2024**, *13*, e12400. [[CrossRef](#)] [[PubMed](#)]
75. Mora, S.; Otvos, J.D.; Rifai, N.; Rosenson, R.S.; Buring, J.E.; Ridker, P.M. Lipoprotein Particle Profiles by Nuclear Magnetic Resonance Compared With Standard Lipids and Apolipoproteins in Predicting Incident Cardiovascular Disease in Women. *Circulation* **2009**, *119*, 931–939. [[CrossRef](#)] [[PubMed](#)]
76. György, B.; Módos, K.; Pállinger, E.; Pálóczi, K.; Pásztói, M.; Misják, P.; Deli, M.A.; Sipos, A.; Szalai, A.; Voszka, I.; et al. Detection and isolation of cell-derived microparticles are compromised by protein complexes resulting from shared biophysical parameters. *Blood* **2011**, *117*, e39–e48. [[CrossRef](#)] [[PubMed](#)]
77. Buzas, E.I.; Toth, E.A.; Sodar, B.W.; Szabo-Taylor, K.E. Molecular interactions at the surface of extracellular vesicles. *Semin. Immunopathol.* **2018**, *40*, 453–464. [[CrossRef](#)] [[PubMed](#)]
78. Tóth, E.Á.; Turiák, L.; Visnovitz, T.; Cserép, C.; Mázló, A.; Sódar, B.W.; Försönits, A.I.; Petővári, G.; Sebestyén, A.; Komlósi, Z.; et al. Formation of a protein corona on the surface of extracellular vesicles in blood plasma. *J. Extracell. Vesicles* **2021**, *10*, e12140. [[CrossRef](#)]
79. Zhang, L.; Song, J.; Cavigiolio, G.; Ishida, B.Y.; Zhang, S.; Kane, J.P.; Weisgraber, K.H.; Oda, M.N.; Rye, K.A.; Pownall, H.J.; et al. Morphology and structure of lipoproteins revealed by an optimized negative-staining protocol of electron microscopy. *J. Lipid Res.* **2011**, *52*, 175–184. [[CrossRef](#)]
80. Sui, X.; Arlt, H.; Brock, K.P.; Lai, Z.W.; DiMaio, F.; Marks, D.S.; Liao, M.; Farese, R.V.; Walther, T.C. Cryo-electron microscopy structure of the lipid droplet-formation protein seipin. *J. Cell Biol.* **2018**, *217*, 4080–4091. [[CrossRef](#)]
81. Uršič, B.; Vozel, D.; Šuštar, V.; Kocjančič, B.; Dolinar, D.; Kralj-Iglič, V. Extracellular vesicles from platelet-rich plasma as conveyors of regeneration potential in orthopedics. *J. Hematol. Thromboembolic Dis.* **2014**, *2*, 5. [[CrossRef](#)]
82. Troha, K.; Vozel, D.; Arko, M.; Bedina Zavec, A.; Dolinar, D.; Hočevar, M.; Jan, Z.; Kisovec, M.; Kocjančič, B.; Pađen, L.; et al. Autologous Platelet and Extracellular Vesicle-Rich Plasma as Therapeutic Fluid: A Review. *Int. J. Mol. Sci.* **2023**, *24*, 3420. [[CrossRef](#)]
83. Chamouard, P.; Desprez, D.; Hugel, B.; Kunzelmann, C.; Gidon-Jeangirard, C.; Lessard, M.; Baumann, R.; Freyssinet, J.M.; Grunebaum, L. Circulating cell-derived microparticles in Crohn's disease. *Dig. Dis. Sci.* **2005**, *50*, 574–580. [[CrossRef](#)]
84. Andoh, A.; Tsujikawa, T.; Hata, K.; Araki, Y.; Kitoh, K.; Sasaki, M.; Yoshida, T.; Fujiyama, Y. Elevated circulating platelet-derived microparticles in patients with active inflammatory bowel disease. *Am. J. Gastroenterol.* **2005**, *100*, 2042–2048. [[CrossRef](#)]
85. Pamuk, G.E.; Vural, O.; Turgut, B.; Demir, M.; Umit, H.; Tezel, A. Increased circulating platelet-neutrophil, platelet-monocyte complexes, and platelet activation in patients with ulcerative colitis: A comparative study. *Am. J. Hematol.* **2006**, *81*, 753–759. [[CrossRef](#)] [[PubMed](#)]
86. Palkovits, J.; Novacek, G.; Kollars, M.; Hron, G.; Osterode, W.; Quehenberger, P.; Kyrle, P.A.; Vogelsang, H.; Reinisch, W.; Papay, P.; et al. Tissue factor exposing microparticles in inflammatory bowel disease. *J. Crohn's Colitis* **2013**, *7*, 222–229. [[CrossRef](#)] [[PubMed](#)]
87. Leonetti, D.; Reimund, J.M.; Tesse, A.; Viennot, S.; Martinez, M.C.; Bretagne, A.L.; Andriantsitohaina, R. Circulating microparticles from Crohn's disease patients cause endothelial and vascular dysfunctions. *PLoS ONE* **2013**, *8*, e73088. [[CrossRef](#)]
88. Tziatzios, G.; Polymeros, D.; Spathis, A.; Triantafyllou, M.; Gkolfakis, P.; Karakitsos, P.; Dimitriadis, G.; Triantafyllou, K. Increased levels of circulating platelet derived microparticles in Crohn's disease patients. *Scand. J. Gastroenterol.* **2016**, *51*, 1184–1192. [[CrossRef](#)] [[PubMed](#)]
89. Xiong, Y.; Lou, P.; Xu, C.; Han, B.; Liu, J.; Gao, J. Emerging role of extracellular vesicles in veterinary practice: Novel opportunities and potential challenges. *Front. Vet. Sci.* **2024**, *11*, 1335107. [[CrossRef](#)] [[PubMed](#)]
90. Lucien, F.; Gustafson, D.; Lenassi, M.; Li, B.; Teske, J.J.; Boilard, E.; von Hohenberg, K.C.; Falcón-Perez, J.M.; Gualerzi, A.; Reale, A.; et al. MIBlood-EV: Minimal information to enhance the quality and reproducibility of blood extracellular vesicle research. *J. Extracell. Vesicles* **2023**, *12*, 12385. [[CrossRef](#)]
91. Yurdakul, C.; Avci, O.; Matlock, A.; Devaux, A.J.; Quintero, M.V.; Ozbay, E.; Davey, R.A.; Connor, J.H.; Karl, W.C.; Tian, L.; et al. High-Throughput, High-Resolution Interferometric Light Microscopy of Biological Nanoparticles. *ACS Nano* **2020**, *14*, 2002–2013. [[CrossRef](#)]
92. Turkki, V.; Alppila, E.; Ylä-Herttua, S.; Lesch, H.P. Experimental Evaluation of an Interferometric Light Microscopy Particle Counter for Titering and Characterization of Virus Preparations. *Viruses* **2021**, *13*, 939. [[CrossRef](#)]

93. Spasovski, V.; Romolo, A.; Zagorc, U.; Arrigler, V.; Kisovec, M.; Bedina Zavec, A.; Arko, M.; Molnár, A.; Schlosser, G.; Iglič, A.; et al. Characterization of Nanohybridosomes from Lipids and Spruce Homogenate Containing Extracellular Vesicles. *Int. J. Nanomed.* **2024**, *19*, 1709–1721. [[CrossRef](#)]
94. Sabbagh, Q.; André-Grégoire, G.; Alves-Nicolau, C.; Dupont, A.; Bidère, N.; Jouglar, E.; Guével, L.; Frénel, J.S.; Gavard, J. The von Willebrand factor stamps plasmatic extracellular vesicles from glioblastoma patients. *Sci. Rep.* **2021**, *11*, 22792. [[CrossRef](#)]
95. Jeran, M.; Romolo, A.; Spasovski, V.; Hočevár, M.; Novak, U.; Štukelj, R.; Šuštar, V.; Kisovec, M.; Bedina Zavec, A.; Kogej, K.; et al. Small Cellular Particles from European Spruce Needle Homogenate. *Int. J. Mol. Sci.* **2023**, *24*, 4349. [[CrossRef](#)] [[PubMed](#)]
96. Kashkanova, A.D.; Blessing, M.; Gemeinhardt, A.; Soulat, D.; Sandoghdar, V. Precision size and refractive index analysis of weakly scattering nanoparticles in polydispersions. *Nat. Methods* **2022**, *19*, 586–593. [[CrossRef](#)] [[PubMed](#)]
97. Buntsma, N.C.; Shahsavari, M.; Gašević, A.; Nieuwland, R.; van Leeuwen, T.G.; van der Pol, E. Preventing swarm detection in extracellular vesicle flow cytometry: A clinically applicable procedure. *Res. Pr. Thromb. Haemost.* **2023**, *7*, 100171. [[CrossRef](#)] [[PubMed](#)]
98. Stanly, C.; Alfieri, M.; Ambrosone, A.; Leone, A.; Fiume, I.; Pocsfalvi, G. Grapefruit-Derived Micro and Nanovesicles Show Distinct Metabolome Profiles and Anticancer Activities in the A375 Human Melanoma Cell Line. *Cells* **2020**, *9*, 2722. [[CrossRef](#)] [[PubMed](#)]
99. Pocsfalvi, G.; Stanly, C.; Vilasi, A.; Fiume, I.; Capasso, G.; Turiák, L.; Buzas, E.I.; Vékey, K. Mass spectrometry of extracellular vesicles. *Mass Spectrom. Rev.* **2016**, *35*, 3–21. [[CrossRef](#)]
100. Garza, A.P.; Wider-Eberspächer, E.; Morton, L.; van Ham, M.; Pallinger, E.; Buzas, E.; Jansch, L.; Dunay, I.R. Proteomic analysis of plasma-derived extracellular vesicles: Pre- and postprandial comparisons. *Sci. Rep.* **2024**, *14*, 23032. [[CrossRef](#)]
101. Schlosser, G.; Molnár, A.; Papp, D.; Gellén, G.; Virág, D.; Ludányi, K.; Dalmadi Kiss, B.; Arko, M.; Iglič, A.; Svete Nemeč, A.; et al. Omics Mass Spectrometry Analysis of Canine Plasma. *Proc. Socrat. Lect.* **2024**, *10*, 67–72. [[CrossRef](#)]

**Disclaimer/Publisher’s Note:** The statements, opinions and data contained in all publications are solely those of the individual author(s) and contributor(s) and not of MDPI and/or the editor(s). MDPI and/or the editor(s) disclaim responsibility for any injury to people or property resulting from any ideas, methods, instructions or products referred to in the content.